

A mortar method for energy-momentum conserving schemes in frictionless dynamic contact problems

Christian Hesch and Peter Betsch^{*,†}

*Chair of Computational Mechanics, Department of Mechanical Engineering, University of Siegen,
Siegen, Germany*

SUMMARY

In the present work the mortar method is applied to planar large deformation contact problems without friction. In particular, the proposed form of the mortar contact constraints is invariant under translations and rotations. These invariance properties lay the foundation for the design of energy-momentum time-stepping schemes for contact–impact problems. The iterative solution procedure is embedded into an active set algorithm. Lagrange multipliers are used to enforce the mortar contact constraints. The solution of generalized saddle point systems is circumvented by applying the discrete null space method. Numerical examples demonstrate the robustness and enhanced numerical stability of the newly developed energy-momentum scheme. Copyright © 2008 John Wiley & Sons, Ltd.

Received 25 April 2008; Revised 6 August 2008; Accepted 6 August 2008

KEY WORDS: solids; contact; finite element method; time integration; energy conserving; mortar method

1. INTRODUCTION

The present work deals with the development of finite element methods for two-dimensional large deformation contact problems without friction. In particular, we aim at conserving time-stepping schemes for contact–impact problems. To achieve this, we make use of the notion of a discrete gradient in the sense of Gonzalez [1, 2] for the evaluation of the discrete contact forces. In Betsch and Hesch [3], this approach has been successfully applied to the node-to-segment (NTS) contact description. The NTS method is currently the prevalent contact formulation in finite element analysis, see the books by Laursen [4] and Wriggers [5].

However, the NTS method has well-known pitfalls such as the lack of general patch test passage and robustness issues arising especially in large deformation problems. To remedy the drawbacks of the NTS method, mortar contact formulations have been devised in recent years, see, for example,

*Correspondence to: Peter Betsch, Chair of Computational Mechanics, Department of Mechanical Engineering, University of Siegen, Siegen, Germany.

†E-mail: betsch@imr.mb.uni-siegen.de

McDevitt and Laursen [6], Puso and Laursen [7], Hübner and Wohlmuth [8], Yang *et al.* [9], Fischer and Wriggers [10], Brunssen *et al.* [11], Hartmann *et al.* [12], and Puso *et al.* [13]. In contrast to the collocation-type description of the contact constraints in the NTS method, the mortar approach relies on an integral formulation of the contact constraints. The weak enforcement of the contact constraints in the mortar formulation is well suited to cope with the faceted representation of the contacting surfaces typically arising in the finite element description of deformable-to-deformable contact problems.

It is now well established that energy-momentum conserving time-stepping schemes and energy-decaying variants thereof provide enhanced numerical stability for applications in non-linear structural dynamics and elastodynamics. It is thus not surprising that a lot of research effort has been spent to extend the energy-momentum approach to coupled problems such as flexible multibody dynamics (see, for example, G eradin and Cardona [14, Chapter 12] and Leyendecker *et al.* [15]) and contact-impact problems, see Laursen [4, Chapter 7]. In this connection, it is interesting to note that conserving time-stepping schemes for large deformation contact-impact problems have been developed exclusively within the framework of the NTS method, see, for example, Laursen and Chawla [16], Armero and Pet ocz [17], Laursen and Love [18], Hauret and Le Tallec [19] and Haikal and Hjeltnad [20].

So far energy-momentum schemes for large deformation contact-impact problems have not been developed within the framework of the mortar method. In a recent paper, Hartmann *et al.* [12] obtain algorithmic energy conservation for their mortar contact description by applying the approach proposed by Laursen and Love [18]. However, similar to all of the above-mentioned works on mortar contact methods, the semi-discrete contact formulation [12] is not invariant under rotations and thus algorithmic conservation of angular momentum is not addressed. The lack of rotational invariance in previous mortar contact approaches can be traced back to simplifying assumptions in the formulation of the discrete contact forces, as pointed out by Puso and Laursen [7, Section 2.2]. Thus the resulting semi-discrete mortar contact formulations do not inherit conservation of angular momentum from the underlying continuous description.

An outline of the present work is as follows. After a short summary of the continuous two-body contact problem (Section 2), we start from a formulation of the mortar contact constraints, which is invariant under translations and rotations (Section 3). Consequently, conservation of linear and angular momentum are preserved under discretization. Guided by our previous developments within the framework of the NTS method (see [3]), Cauchy's representation theorem is exploited to recast the mortar contact constraints in terms of quadratic invariants. This paves the way for the energy-momentum conserving discretization in time (Section 4). The use of Lagrange multipliers for the enforcement of the mortar contact constraints leads to a generalized saddle point problem that has to be solved in each step of the iterative solution procedure. The Lagrange multipliers can be eliminated by applying the discrete null space method (Section 5). In addition to the size-reduction, this approach yields an improved conditioning (independent of the time-step) of the algebraic system to be solved. Representative numerical examples are presented in Section 6. Eventually, conclusions are drawn in Section 7.

2. THE TWO-BODY LARGE DEFORMATION CONTACT PROBLEM

This section provides a short outline of the two-body contact problem under consideration. We refer to the books by Laursen [4] and Wriggers [5] for more background on the subject.

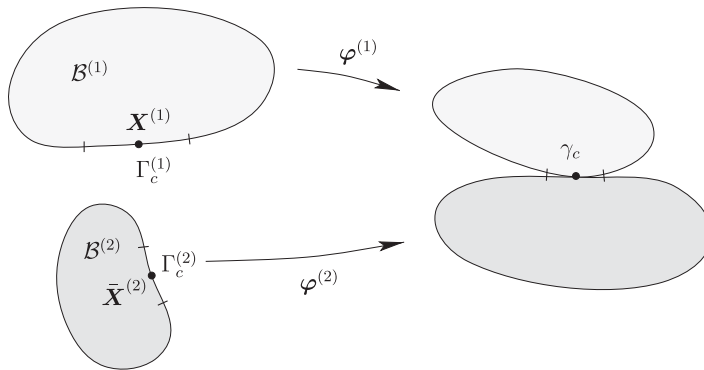


Figure 1. The two-body large deformation contact problem.

We focus our attention on the planar two-body contact problem depicted schematically in Figure 1. For each body (i) , the deformation mapping $\boldsymbol{\varphi}^{(i)}(\mathbf{X}^{(i)}, t)$ maps material points $\mathbf{X}^{(i)}$ belonging to the reference configuration $\mathcal{B}^{(i)} \subset \mathbb{R}^2$ to their current placement at time t . The boundary $\Gamma^{(i)}$ of the reference configuration $\mathcal{B}^{(i)}$ is subdivided into the subdomains $\Gamma_u^{(i)}$ and $\Gamma_\sigma^{(i)}$, where Dirichlet and Neumann boundary conditions are specified, and $\Gamma_c^{(i)}$, where contact may occur. These subdomains have to satisfy

$$\Gamma_u^{(i)} \cup \Gamma_\sigma^{(i)} \cup \Gamma_c^{(i)} = \Gamma^{(i)} \tag{1}$$

and

$$\Gamma_u^{(i)} \cap \Gamma_\sigma^{(i)} = \Gamma_u^{(i)} \cap \Gamma_c^{(i)} = \Gamma_\sigma^{(i)} \cap \Gamma_c^{(i)} = \emptyset \tag{2}$$

Contact between the two bodies occurs, if

$$\boldsymbol{\varphi}^{(1)}(\mathbf{X}^{(1)}, t) = \boldsymbol{\varphi}^{(2)}(\bar{\mathbf{X}}^{(2)}, t) \tag{3}$$

where $\bar{\mathbf{X}}^{(2)}$ is the material contact point for $\mathbf{X}^{(1)}$ at time t .

To write down the principle of virtual work we first introduce the space of admissible functions as

$$\mathbb{Q} = \{ \boldsymbol{\varphi}^{(i)} : \mathcal{B}^{(i)} \rightarrow \mathbb{R}^2 \mid \boldsymbol{\varphi}^{(i)} = \bar{\boldsymbol{\varphi}}^{(i)} \text{ in } \Gamma_u^{(i)} \} \tag{4}$$

where $\bar{\boldsymbol{\varphi}}^{(i)}$ denotes the prescribed displacements. In addition to that, the space of the admissible variations is given by

$$\mathbb{V} = \{ \delta \boldsymbol{\varphi}^{(i)} : \mathcal{B}^{(i)} \rightarrow \mathbb{R}^2 \mid \delta \boldsymbol{\varphi}^{(i)} = \mathbf{0} \text{ in } \Gamma_u^{(i)} \} \tag{5}$$

For the large deformation two-body contact problem, the principle of virtual work can be expressed in the form

$$\sum_{i=1}^2 (G^{(i), \text{dyn}} + G^{(i), \text{int}} - G^{(i), \text{ext}} - G^{(i), \text{c}}) = 0 \tag{6}$$

Here, the contribution of the inertia terms is given by

$$G^{(i), \text{dyn}}(\boldsymbol{\varphi}^{(i)}, \delta \boldsymbol{\varphi}^{(i)}) = \int_{\mathcal{B}^{(i)}} \delta \boldsymbol{\varphi}^{(i)} \cdot \rho_{\text{R}} \ddot{\boldsymbol{\varphi}}^{(i)} \, dV \tag{7}$$

where ρ_R is the reference mass density and a superposed dot denotes differentiation with respect to time. The virtual work arising from the internal forces reads as

$$G^{(i),\text{int}}(\boldsymbol{\varphi}^{(i)}, \delta\boldsymbol{\varphi}^{(i)}) = \int_{\mathcal{B}^{(i)}} \nabla(\delta\boldsymbol{\varphi}^{(i)}) : \mathbf{P}^{(i)} \, dV \tag{8}$$

where $\mathbf{P}^{(i)}$ denotes the first Piola–Kirchhoff stress tensor. Moreover, the virtual work arising from the external forces is given by

$$G^{(i),\text{ext}}(\boldsymbol{\varphi}^{(i)}, \delta\boldsymbol{\varphi}^{(i)}) = \int_{\mathcal{B}^{(i)}} \rho_R \mathbf{B}^{(i)} \cdot \delta\boldsymbol{\varphi}^{(i)} \, dV + \int_{\Gamma_c^{(i)}} \bar{\mathbf{T}}^{(i)} \cdot \delta\boldsymbol{\varphi} \, d\Gamma \tag{9}$$

where $\mathbf{B}^{(i)}$ denotes the applied body forces and $\bar{\mathbf{T}}^{(i)}$ denotes the prescribed tractions. The virtual work associated with the contact tractions is given by

$$G^c = \sum_{i=1}^2 G^{(i),c} \tag{10}$$

with

$$G^{(i),c}(\boldsymbol{\varphi}^{(i)}, \delta\boldsymbol{\varphi}^{(i)}) = \int_{\gamma_c^{(i)}} \delta\boldsymbol{\varphi}^{(i)} \cdot \mathbf{t}^{(i)} \, d\gamma \tag{11}$$

Here, $\gamma_c^{(i)}$ is the current configuration of $\Gamma_c^{(i)}$ and $\mathbf{t}^{(i)}$ is the Cauchy contact traction. Performing the summation in (10) and substituting $-\mathbf{t}^{(1)}$ for $\mathbf{t}^{(2)}$, we obtain

$$G^c = \int_{\gamma_c^{(1)}} \mathbf{t}^{(1)} \cdot (\delta\boldsymbol{\varphi}^{(1)}(\mathbf{X}^{(1)}, t) - \delta\boldsymbol{\varphi}^{(2)}(\bar{\mathbf{X}}^{(2)}, t)) \, d\gamma \tag{12}$$

In anticipation of the spatial discretization, $\gamma_c^{(1)}$ is called the non-mortar (or slave) side. Similarly, $\gamma_c^{(2)}$ is referred to as the mortar (or master) side. In the case of frictionless contact only the normal component of $\mathbf{t}^{(1)}$, defined by $\mathbf{t}^{(1)} \cdot \mathbf{v}^{(1)} =: \lambda$ is non-zero. In this connection, $\mathbf{v}^{(1)}$ is the outward unit normal to $\gamma_c^{(1)}$. Accordingly, $\mathbf{t}^{(1)} = \lambda \mathbf{v}^{(1)}$, so that Equation (12) can be rewritten as

$$G^c = \int_{\gamma_c^{(1)}} (\lambda \mathbf{v}^{(1)})(\mathbf{X}^{(1)}, t) \cdot (\delta\boldsymbol{\varphi}^{(1)}(\mathbf{X}^{(1)}, t) - \delta\boldsymbol{\varphi}^{(2)}(\bar{\mathbf{X}}^{(2)}, t)) \, d\gamma \tag{13}$$

3. DISCRETIZATION IN SPACE

Concerning the discretization in space we apply displacement-based finite elements [21]. Accordingly, standard polynomial approximations to \mathbb{Q} are used, which can be written in the form

$$\boldsymbol{\varphi}^{(i),h} = \sum_{A \in \omega^{(i)}} N^A(\mathbf{X}^{(i)}) \mathbf{q}_A^{(i)} \tag{14}$$

Here, $N^A : \mathcal{B}^{(i)} \rightarrow \mathbb{R}$ are global shape functions associated with nodes $A \in \omega^{(i)} = \{1, \dots, n_{\text{node}}^{(i)}\}$ corresponding to the isoparametric description of $\mathcal{B}^{(i)}$. Moreover, $\mathbf{q}_A^{(i)}(t) = \boldsymbol{\varphi}^{(i),h}(\mathbf{X}_A^{(i)}, t)$ is the current position vector of the nodal point $\mathbf{X}_A^{(i)} \in \mathcal{B}^{(i)}$. In the present work we restrict our attention

to planar problems and bi-linear shape functions. The configuration of each semi-discrete flexible body is characterized by its configuration vector

$$\mathbf{q}^{(i)}(t) = \begin{bmatrix} \mathbf{q}_1^{(i)}(t) \\ \vdots \\ \mathbf{q}_{n_{\text{node}}}^{(i)}(t) \end{bmatrix} \tag{15}$$

For the two-body contact problem under consideration the configuration of the complete semi-discrete system is given by

$$\mathbf{q}(t) = \begin{bmatrix} \mathbf{q}^{(1)}(t) \\ \mathbf{q}^{(2)}(t) \end{bmatrix} \tag{16}$$

The discretized versions of the deformation gradient and the deformation tensor are given by

$$\mathbf{F}^{(i),h} = \frac{\partial \boldsymbol{\varphi}^{(i),h}}{\partial \mathbf{X}^{(i)}} = \sum_{A \in \omega^{(i)}} \mathbf{q}_A^{(i)} \otimes \nabla N^A(\mathbf{X}^{(i)}) \tag{17}$$

and

$$\mathbf{C}^{(i),h} = \sum_{A, B \in \omega^{(i)}} \mathbf{q}_A^{(i)} \cdot \mathbf{q}_B^{(i)} \nabla N^A(\mathbf{X}^{(i)}) \otimes \nabla N^B(\mathbf{X}^{(i)}) \tag{18}$$

The discrete counterpart of (7) can be written as

$$G^{(i),\text{dyn}}(\boldsymbol{\varphi}^{(i),h}, \delta \boldsymbol{\varphi}^{(i),h}) = \int_{\mathcal{B}^{(i)}} \delta \boldsymbol{\varphi}^{(i),h} \cdot \rho_{\mathbf{R}} \ddot{\boldsymbol{\varphi}}^{(i),h} dV = \sum_{A, B \in \omega^{(i)}} \delta \mathbf{q}_A^{(i)} \cdot M^{AB} \ddot{\mathbf{q}}_B^{(i)} \tag{19}$$

where the coefficients of the consistent mass matrix

$$M^{AB} = \int_{\mathcal{B}} \rho_{\mathbf{R}} N^A N^B dV \tag{20}$$

have been introduced. Moreover, $\delta \mathbf{q}_A^{(i)}$ denotes the standard variation of the nodal values in (14). The kinetic energy pertaining to each semi-discrete body assumes the form

$$T^{(i)} = \sum_{A, B \in \omega^{(i)}} \frac{1}{2} \dot{\mathbf{q}}_A^{(i)} \cdot M^{AB} \dot{\mathbf{q}}_B^{(i)} \tag{21}$$

Correspondingly, the total kinetic energy of the two-body system under consideration can be written as

$$T = \frac{1}{2} \dot{\mathbf{q}} \cdot \mathbf{M} \dot{\mathbf{q}} \tag{22}$$

where the system velocity vector $\dot{\mathbf{q}}$ follows from differentiating (16) with respect to time, and the system mass matrix \mathbf{M} contains the elements (20), arranged consistently with the partitioning of \mathbf{q} in (16).

The discrete counterpart of expression (8) for the internal virtual work can be written as

$$G^{(i),\text{int}}(\boldsymbol{\varphi}^{(i),h}, \delta\boldsymbol{\varphi}^{(i),h}) = \sum_{A,B \in \omega^{(i)}} \delta\mathbf{q}_A^{(i)} \cdot \mathbf{q}_B^{(i)} \int_{\mathcal{B}^{(i)}} \nabla N^A(\mathbf{X}^{(i)}) \cdot \mathbf{S}^{(i)} \nabla N^B(\mathbf{X}^{(i)}) dV \quad (23)$$

where $\mathbf{S} = 2\partial W/\partial \mathbf{C}$ denotes the second Piola–Kirchhoff stress tensor and $W(\mathbf{C})$ denotes the stored energy function. The strain energy of each body can now be written in the form

$$V^{(i),\text{int}}(\mathbf{q}^{(i)}) = \int_{\mathcal{B}^{(i)}} W(\mathbf{C}^{(i),h}) dV \quad (24)$$

Under the assumption that the external virtual work can be derived from a potential energy function as

$$V^{(i),\text{ext}}(\mathbf{q}^{(i)}) = \sum_{A \in \omega^{(i)}} \mathbf{q}_A^{(i)} \cdot \left(\int_{\mathcal{B}^{(i)}} N^A \mathbf{B}^{(i)} dV + \int_{\Gamma_\sigma^{(i)}} N^A \bar{\mathbf{T}}^{(i)} d\Gamma \right) \quad (25)$$

the discrete counterpart of (9) can be written as

$$G^{(i),\text{ext}}(\boldsymbol{\varphi}^{(i),h}, \delta\boldsymbol{\varphi}^{(i),h}) = \nabla V^{(i),\text{ext}}(\mathbf{q}^{(i)}) \cdot \delta\mathbf{q}^{(i)} \quad (26)$$

Now the semi-discrete formulation of the two-body system at hand can be associated with a potential energy function of the form

$$V(\mathbf{q}) = V^{\text{int}}(\mathbf{q}) + V^{\text{ext}}(\mathbf{q}) = \sum_{i=1}^2 (V^{(i),\text{int}}(\mathbf{q}^{(i)}) + V^{(i),\text{ext}}(\mathbf{q}^{(i)})) \quad (27)$$

Moreover, we can introduce an augmented potential function [3] as

$$V_\lambda(\mathbf{q}) = V(\mathbf{q}) + \sum_{A \in \bar{\omega}^{(1)}} \lambda_A \Phi^A(\mathbf{q}) \quad (28)$$

The last term in the above expression can be viewed as potential function associated with the contact constraints.[‡] In the following, we shall focus on the specific potential function arising from a mortar contact formulation. In particular, the mortar contact constraints $\Phi^A(\mathbf{q})$ will be specified next.

3.1. Mortar contact constraints

In contrast to the collocation-type formulation of the contact constraints in the NTS approach, the mortar concept relies on the weak enforcement of the contact constraints. Following Puso and Laursen [7, Section 2], the potential function of the normal contact constraints pertaining to the mortar method can be derived from an integral form of the contact complementarity condition. Accordingly,

$$\int_{\gamma_c^{(1),h}} (\lambda^h \mathbf{v}^h)(\mathbf{X}^{(1)}, t) \cdot (\boldsymbol{\varphi}^{(1),h}(\mathbf{X}^{(1)}, t) - \boldsymbol{\varphi}^{(2),h}(\bar{\mathbf{X}}^{(2)}, t)) d\gamma =: \sum_{A \in \bar{\omega}^{(1)}} \lambda_A \Phi^A(\mathbf{q}) \quad (29)$$

[‡]We do not dwell on constraints due to Dirichlet boundary conditions that can be accommodated in a standard fashion.

Here, the description of the discrete boundaries $\gamma_c^{(1),h}$ and $\gamma_c^{(2),h}$ follows from the space discretization. Thus

$$\boldsymbol{\varphi}^{(1),h}(\mathbf{X}^{(1)}, t) = \sum_{B \in \bar{\omega}^{(1)}} N^B(\mathbf{X}^{(1)}) \mathbf{q}_B^{(1)}(t) \quad \text{for } \mathbf{X}^{(1)} \in \Gamma_C^{(1),h} \tag{30}$$

$$\boldsymbol{\varphi}^{(2),h}(\mathbf{X}^{(2)}, t) = \sum_{C \in \bar{\omega}^{(2)}} N^C(\mathbf{X}^{(2)}) \mathbf{q}_C^{(2)}(t) \quad \text{for } \mathbf{X}^{(2)} \in \Gamma_C^{(2),h} \tag{31}$$

where $\bar{\omega}^{(1)} \subset \omega^{(1)}$ and $\bar{\omega}^{(2)} \subset \omega^{(2)}$ denote the set of potential contact nodes lying on $\gamma_c^{(1),h}$ and $\gamma_c^{(2),h}$, respectively. The approximation of λ^h is given by

$$\lambda^h(\mathbf{X}^{(1)}, t) = \sum_{A \in \bar{\omega}^{(1)}} N^A(\mathbf{X}^{(1)}) \lambda_A(t) \tag{32}$$

where, as in (30), the shape functions $N^A(\mathbf{X}^{(1)})$, $A \in \bar{\omega}^{(1)}$, are inherited from the non-mortar side. Inserting Equations (30)–(32) into Equation (29) yields the mortar contact constraints

$$\begin{aligned} \Phi^A(\mathbf{q}) &= \sum_{B \in \bar{\omega}^{(1)}} \mathbf{q}_B^{(1)} \cdot \int_{\gamma_c^{(1),h}} \mathbf{v}^h N^A(\mathbf{X}^{(1)}) N^B(\mathbf{X}^{(1)}) d\gamma \\ &\quad - \sum_{C \in \bar{\omega}^{(2)}} \mathbf{q}_C^{(2)} \cdot \int_{\gamma_c^{(1),h}} \mathbf{v}^h N^A(\mathbf{X}^{(1)}) N^C(\bar{\mathbf{X}}^{(2)}) d\gamma \end{aligned} \tag{33}$$

Note that the integration in (33) has to be performed across the current contact domain. For that purpose, a suitable segmentwise procedure will be treated next.

3.2. Elementwise calculation of the mortar contact constraints

To perform the integration along the discrete boundary $\gamma_c^{(1),h}$, the notion of a contact segment shall be utilized. Originally, contact segments have been introduced by Simo *et al.* [22] to take into account the kinematics of the contact between two discretized bodies. Similar segmentation procedures have been devised by Papadopoulos and Taylor [23], Zavarise and Wriggers [24], McDevitt and Laursen [6] and Yang *et al.* [9].

With regard to the above treatment it is obvious that the individual constraint functions $\Phi^A(\mathbf{q})$ correspond to nodal points lying on the non-mortar side, i.e. $A \in \bar{\omega}^{(1)}$. The constraint functions may be arranged in a vector of constraint functions $\Phi(\mathbf{q})$, such that

$$\sum_{A \in \bar{\omega}^{(1)}} \lambda_A \Phi^A(\mathbf{q}) = \boldsymbol{\lambda} \cdot \Phi(\mathbf{q}) \tag{34}$$

The vector of constraint functions can be computed by assembling the contributions of the (one-dimensional) elements $e \in \bar{\varepsilon}^{(1)}$, where $\bar{\varepsilon}^{(1)}$ denotes the set of elements representing the non-mortar side $\gamma_c^{(1),h}$ (see Figure 2). In the present case, $\gamma_c^{(1),h}$ corresponds to a polygon composed of two-node elements $e \in \bar{\varepsilon}^{(1)}$.

In the sequel, we shall focus on a representative element $e \in \bar{\varepsilon}^{(1)}$ with local node numbers $\alpha = 1, 2$. The connection between local and global node numbers is stored in the location array LM, such that $A = \text{LM}(\alpha, e)$, for $A \in \bar{\omega}^{(1)}$, $\alpha \in \{1, 2\}$, and $e \in \bar{\varepsilon}^{(1)}$. Once the element contributions

$$\Phi_e = \begin{bmatrix} \Phi_e^1 \\ \Phi_e^2 \end{bmatrix} \tag{35}$$

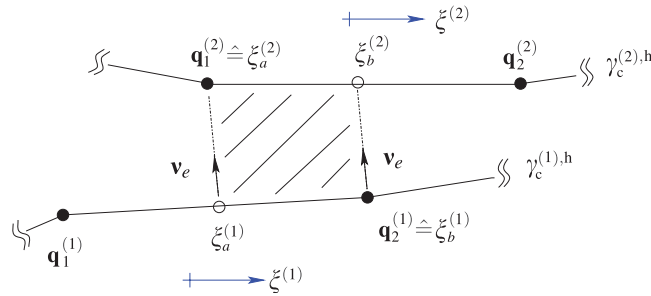


Figure 2. Representative mortar segment with element boundaries on the discrete non-mortar side $\gamma_c^{(1),h}$ and mortar side $\gamma_c^{(2),h}$.

have been computed they can be added to the appropriate location in the vector Φ . That is,

$$\Phi = \mathbf{A} \Phi_e \tag{36}$$

where \mathbf{A} denotes the standard assembly operator (see, for example, [21]). On the element level, the evaluation of the integrals in (33) can be accomplished by resorting to the above-mentioned segmentation procedure. To this end, we consider a representative mortar segment depicted in Figure 2. The relevant nodal position vectors lying on the boundaries of the two opposing elements may be collected in the vector

$$\mathbf{q}_{\text{seg}} = [\mathbf{q}_1^{(1)\text{T}} \quad \mathbf{q}_2^{(1)\text{T}} \quad \mathbf{q}_1^{(2)\text{T}} \quad \mathbf{q}_2^{(2)\text{T}}]^\text{T} \in \mathbb{R}^8 \tag{37}$$

where local node numbers have been used to denote the position vectors $\mathbf{q}_1^{(1)}, \mathbf{q}_2^{(1)} \in \gamma_c^{(1),h}$ and $\mathbf{q}_1^{(2)}, \mathbf{q}_2^{(2)} \in \gamma_c^{(2),h}$. To each mortar segment there corresponds four coordinates $\xi_a^{(1)}, \xi_b^{(1)}, \xi_a^{(2)}$, and $\xi_b^{(2)}$, where $\xi^{(1)}, \xi^{(2)} \in [-1, 1]$ are local coordinates for the parametrization of the element boundaries on the non-mortar and mortar sides, respectively. For each segment a linear mapping $[-1, 1] \ni \eta \rightarrow \xi^{(i)}$ of the form

$$\xi^{(i)}(\eta) = \frac{1}{2}(1 - \eta)\xi_a^{(i)} + \frac{1}{2}(1 + \eta)\xi_b^{(i)} \tag{38}$$

is introduced. The interpolations (30)–(32) can now be recast in the form

$$\begin{aligned} \lambda^h(\eta, t) &= \sum_{\alpha=1}^2 N^\alpha(\xi^{(1)}(\eta)) \lambda_\alpha(t) \\ \Phi^{(1),h}(\eta, t) &= \sum_{\beta=1}^2 N^\beta(\xi^{(1)}(\eta)) \mathbf{q}_\beta^{(1)}(t) \\ \Phi^{(2),h}(\eta, t) &= \sum_{\zeta=1}^2 N^\zeta(\xi^{(2)}(\eta)) \mathbf{q}_\zeta^{(2)}(t) \end{aligned} \tag{39}$$

with local shape functions

$$\begin{aligned} N^1(\zeta) &= \frac{1}{2}(1 - \zeta) \\ N^2(\zeta) &= \frac{1}{2}(1 + \zeta) \end{aligned} \tag{40}$$

Now, with regard to Equation (33), on the element level we obtain

$$\Phi_e^\alpha = \bigcup_{\text{seg}} \Phi_{\text{seg}}^\alpha(\mathbf{q}_{\text{seg}}) \tag{41}$$

where the segment contributions[§] are given by

$$\Phi_{\text{seg}}^\alpha(\mathbf{q}_{\text{seg}}) = \mathbf{v}_e \cdot \left\{ \sum_{\beta=1}^2 n_{\text{seg}}^{\alpha\beta,(1)} \mathbf{q}_\beta^{(1)} - \sum_{\zeta=1}^2 n_{\text{seg}}^{\alpha\zeta,(2)} \mathbf{q}_\zeta^{(2)} \right\} \tag{42}$$

In the last equation the mortar integrals assume the form

$$\begin{aligned} n_{\text{seg}}^{\alpha\beta,(1)} &= \int_{-1}^1 N^\alpha(\xi^{(1)}(\eta)) N^\beta(\xi^{(1)}(\eta)) j_{\text{seg}} \, d\eta \\ n_{\text{seg}}^{\alpha\zeta,(2)} &= \int_{-1}^1 N^\alpha(\xi^{(1)}(\eta)) N^\zeta(\xi^{(2)}(\eta)) j_{\text{seg}} \, d\eta \end{aligned} \tag{43}$$

where $d\gamma = j_{\text{seg}} \, d\eta$, with

$$j_{\text{seg}} = \left\| \frac{\partial \boldsymbol{\Phi}^{(1),h}}{\partial \xi^{(1)}} \frac{\partial \xi^{(1)}}{\partial \eta} \right\| \tag{44}$$

Note that, depending on the segmentation procedure, all segment contributions relevant to the element $e \in \bar{\varepsilon}^{(1)}$ have to be taken into account, cf. Equation (41). Moreover, a constant unit outward normal \mathbf{v}_e has been employed for each $e \in \bar{\varepsilon}^{(1)}$. This is slightly different from the use of a nodally averaged normal in Puso and Laursen [7]. We further remark that, for the semi-discrete system under consideration, the virtual work expression (12) can be written as

$$\begin{aligned} G^{\text{c,h}} &= \delta \mathbf{q} \cdot \left\{ \sum_{A \in \bar{\omega}^{(1)}} \lambda_A \nabla \Phi^A(\mathbf{q}) \right\} \\ &= \delta \mathbf{q} \cdot \{ D\boldsymbol{\Phi}^T(\mathbf{q}) \boldsymbol{\lambda} \} \end{aligned} \tag{45}$$

Here, the term in the curly brackets corresponds to the vector of nodal contact forces. Taking into account the elementwise description outlined above, the last equation can also be written as

$$G^{\text{c,h}} = \sum_{e \in \bar{\varepsilon}^{(1)}} \left(\bigcup_{\text{seg}} \delta \mathbf{q}_{\text{seg}} \cdot D\boldsymbol{\Phi}_{\text{seg}}^T(\mathbf{q}_{\text{seg}}) \right) \boldsymbol{\lambda}^e \tag{46}$$

[§]Note that each segment *seg* is always associated with a specific element *e*. However, to avoid notational clumsiness, we refrain from using the notation *seg_e*.

where

$$\boldsymbol{\lambda}^e = \begin{bmatrix} \lambda_1^e \\ \lambda_2^e \end{bmatrix} \tag{47}$$

with $\lambda_\alpha^e = \lambda_A$ for $A = \text{LM}(\alpha, e)$. It is worth noting that in previous works on mortar contact formulations (see [7, 9, 12, 13]) additional simplifying assumptions are commonly incorporated into the contact virtual work. These simplifications typically sacrifice conservation of the angular momentum.

In contrast to these works we retain all the configuration-dependent terms in the virtual work expression (46). Consequently, important conservation properties such as conservation of the angular momentum are preserved by the present finite element approximation in space. Moreover, in the purely static case, consistent linearization yields a symmetric tangent operator.

3.3. Mortar contact constraints and conservation of momentum maps

In this section we present a reparametrization of the mortar contact constraints in terms of quadratic invariants. The advocated reparametrization allows the design of an energy-momentum scheme. In addition to that, it verifies that the present space discretization inherits conservation of the linear and angular momentum from the underlying continuous formulation.

3.3.1. Conservation of the linear and angular momentum. Provided that there are no Dirichlet boundary conditions and no external forces, possible contact interactions between the two-body system do not change the total linear and angular momentum of the system. One way to verify these fundamental features of the continuous system is to choose appropriate substitutions for the variations $\delta\boldsymbol{\varphi}^{(i)}$ in the virtual work (see, for example, Laursen [4, Section 7.2.1]). In the present work, we focus on the contact virtual work. Accordingly, substituting $\delta\boldsymbol{\varphi}^{(i)} = \boldsymbol{\xi}$, where $\boldsymbol{\xi} \in \mathbb{R}^3$ is constant,[¶] into expression (12) for the contact virtual work yields

$$\sum_{i=1}^2 G^{(i),c}(\boldsymbol{\varphi}^{(i)}, \boldsymbol{\xi}) = 0 \tag{48}$$

This result allows conservation of the total linear momentum. Similarly, substitution of $\delta\boldsymbol{\varphi}^{(i)} = \boldsymbol{\xi} \times \boldsymbol{\varphi}^{(i)}$ yields

$$\sum_{i=1}^2 G^{(i),c}(\boldsymbol{\varphi}^{(i)}, \boldsymbol{\xi} \times \boldsymbol{\varphi}^{(i)}) = 0 \tag{49}$$

which allows conservation of the total angular momentum.

If conservation of the linear and angular momentum is to be preserved under discretization, discrete analogues of (48) and (49) have to hold. Similar to the continuous case outlined above,

[¶]Since the present work focuses on planar problems, we identify \mathbb{R}^2 with the orthogonal complement of the canonical basis vector \mathbf{e}_3 in \mathbb{R}^3 . Similarly, in the sequel, a rotation matrix on \mathbb{R}^2 will be taken to be one whose extension to \mathbb{R}^3 is proper orthogonal and leaves \mathbf{e}_3 unchanged.

these analogues can be obtained by inserting into (46) appropriate nodal patterns for $\delta \mathbf{q}_{\text{seg}}$, where $\delta \mathbf{q}_{\text{seg}}$ is given by (37). Accordingly, satisfaction of the relationship

$$\sum_{e \in \bar{e}^{(1)}} \left(\bigcup_{\text{seg}} [\xi^T \ \xi^T \ \xi^T \ \xi^T] D \Phi_{\text{seg}}^T(\mathbf{q}_{\text{seg}}) \right) \lambda^e \stackrel{!}{=} 0 \tag{50}$$

is required for conservation of the total linear momentum, whereas fulfillment of the condition

$$\sum_{e \in \bar{e}^{(1)}} \left(\bigcup_{\text{seg}} [(\xi \times \mathbf{q}_1^{(1)})^T \ (\xi \times \mathbf{q}_2^{(1)})^T \ (\xi \times \mathbf{q}_1^{(2)})^T \ (\xi \times \mathbf{q}_2^{(2)})^T] D \Phi_{\text{seg}}^T(\mathbf{q}_{\text{seg}}) \right) \lambda^e \stackrel{!}{=} 0 \tag{51}$$

allows conservation of the total angular momentum of the semi-discrete system.

3.3.2. *Conservation laws and invariance properties.* According to Noether’s theorem conservation laws are related to invariance properties of the system. For the semi-discrete system under consideration, conservation of the linear and angular momentum can be linked to the invariance of the augmented potential function (28) under translations and rotations, respectively. In particular, conditions (50) and (51) are automatically satisfied if the mortar contact constraints are invariant under translations and rotations, respectively. With regard to the relationships (36), (35) and (41), it suffices to consider in the sequel the segment contributions $\Phi_{\text{seg}}(\mathbf{q}_{\text{seg}}) \in \mathbb{R}^2$ specified by (42).

(i) Translational invariance of the mortar constraints implies that

$$\Phi_{\text{seg}}(\mathbf{q}_1^{(1)} + \varepsilon \xi, \mathbf{q}_2^{(1)} + \varepsilon \xi, \mathbf{q}_1^{(2)} + \varepsilon \xi, \mathbf{q}_2^{(2)} + \varepsilon \xi) = \Phi_{\text{seg}}(\mathbf{q}_1^{(1)}, \mathbf{q}_2^{(1)}, \mathbf{q}_1^{(2)}, \mathbf{q}_2^{(2)}) \tag{52}$$

for arbitrary $\varepsilon \in \mathbb{R}$. Accordingly,

$$\begin{aligned} \mathbf{0} &= \left. \frac{d}{d\varepsilon} \right|_{\varepsilon=0} \Phi_{\text{seg}}(\mathbf{q}_1^{(1)} + \varepsilon \xi, \mathbf{q}_2^{(1)} + \varepsilon \xi, \mathbf{q}_1^{(2)} + \varepsilon \xi, \mathbf{q}_2^{(2)} + \varepsilon \xi) \\ &= D \Phi_{\text{seg}}(\mathbf{q}_{\text{seg}}) \begin{bmatrix} \xi \\ \xi \\ \xi \\ \xi \end{bmatrix} \end{aligned} \tag{53}$$

Thus, provided that $\Phi_{\text{seg}}(\mathbf{q}_{\text{seg}})$ is invariant under translations, condition (50) is automatically fulfilled.

(ii) Rotational invariance of the mortar constraints implies that

$$\begin{aligned} &\Phi_{\text{seg}}(\exp(\varepsilon \hat{\xi}) \mathbf{q}_1^{(1)}, \exp(\varepsilon \hat{\xi}) \mathbf{q}_2^{(1)}, \exp(\varepsilon \hat{\xi}) \mathbf{q}_1^{(2)}, \exp(\varepsilon \hat{\xi}) \mathbf{q}_2^{(2)}) \\ &= \Phi_{\text{seg}}(\mathbf{q}_1^{(1)}, \mathbf{q}_2^{(1)}, \mathbf{q}_1^{(2)}, \mathbf{q}_2^{(2)}) \end{aligned} \tag{54}$$

Here, the exponential map $\exp(\varepsilon \widehat{\xi})$ represents a rotation matrix on \mathbb{R}^2 . Now

$$\begin{aligned} \mathbf{0} &= \left. \frac{d}{d\varepsilon} \right|_{\varepsilon=0} \Phi_{\text{seg}}(\exp(\varepsilon \widehat{\xi}) \mathbf{q}_1^{(1)}, \exp(\varepsilon \widehat{\xi}) \mathbf{q}_2^{(1)}, \exp(\varepsilon \widehat{\xi}) \mathbf{q}_1^{(2)}, \exp(\varepsilon \widehat{\xi}) \mathbf{q}_2^{(2)}) \\ &= D\Phi_{\text{seg}}(\mathbf{q}_{\text{seg}}) \begin{bmatrix} \xi \times \mathbf{q}_1^{(1)} \\ \xi \times \mathbf{q}_2^{(1)} \\ \xi \times \mathbf{q}_1^{(2)} \\ \xi \times \mathbf{q}_2^{(2)} \end{bmatrix} \end{aligned} \tag{55}$$

so that invariance of $\Phi_{\text{seg}}(\mathbf{q}_{\text{seg}})$ under rotations implies satisfaction of condition (51).

3.3.3. *Mortar contact constraints in terms of invariants.* We next show that the mortar contact constraints (42) can be recast in terms of specific invariants. This automatically ensures that the above invariance properties (i) and (ii) are satisfied. To devise appropriate invariants we resort to Cauchy’s representation theorem (see Truesdell and Noll [25, Section 11] or Antman [26, Chapter 8]). Accordingly, if a scalar-valued function

$$\gamma(\mathbf{q}_{\text{seg}}) = \gamma(\mathbf{q}_1^{(1)}, \mathbf{q}_2^{(1)}, \mathbf{q}_1^{(2)}, \mathbf{q}_2^{(2)}) \tag{56}$$

is invariant under the proper orthogonal group, then it depends only on the set of quadratic invariants $\mathbb{I}(\mathbf{q}_{\text{seg}}) = \mathbb{S}(\mathbf{q}_{\text{seg}}) \cup \mathbb{T}(\mathbf{q}_{\text{seg}})$, where

$$\begin{aligned} \mathbb{S}(\mathbf{q}_{\text{seg}}) &= \{\mathbf{y}_\alpha \cdot \mathbf{y}_\beta, 1 \leq \alpha \leq \beta \leq 2, \mathbf{y}_\alpha \in \{\mathbf{q}_\alpha^{(1)}, \mathbf{q}_\alpha^{(2)}\}\} \\ \mathbb{T}(\mathbf{q}_{\text{seg}}) &= \{\det([\mathbf{y}_\alpha, \mathbf{y}_\beta]), 1 \leq \alpha \leq \beta \leq 2, \mathbf{y}_\alpha \in \{\mathbf{q}_\alpha^{(1)}, \mathbf{q}_\alpha^{(2)}\}\} \end{aligned} \tag{57}$$

We now seek for reparametrizations of the mortar contact constraints (42) of the form

$$\Phi_{\text{seg}}^\alpha(\mathbf{q}_{\text{seg}}) = \tilde{\Phi}_{\text{seg}}^\alpha(\boldsymbol{\pi}(\mathbf{q}_{\text{seg}})) \tag{58}$$

for $\alpha = 1, 2$. Here, $\boldsymbol{\pi}(\mathbf{q}_{\text{seg}}) = [\pi_1(\mathbf{q}_{\text{seg}}), \dots, \pi_d(\mathbf{q}_{\text{seg}})]^T$ is the vector of relevant invariants. With regard to Cauchy’s representation theorem the components $\pi_i(\mathbf{q}_{\text{seg}})$, $i = 1, \dots, d$, have to be composed of quadratic invariants specified by $\mathbb{I}(\mathbf{q}_{\text{seg}})$. In addition to that, with regard to (52), translational invariance requires that the invariants also satisfy the condition

$$\pi_i(\mathbf{q}_1^{(1)} + \xi, \mathbf{q}_2^{(1)} + \xi, \mathbf{q}_1^{(2)} + \xi, \mathbf{q}_2^{(2)} + \xi) = \pi_i(\mathbf{q}_1^{(1)}, \mathbf{q}_2^{(1)}, \mathbf{q}_1^{(2)}, \mathbf{q}_2^{(2)}) \tag{59}$$

As indicated in Figure 2, the filled circles correspond to nodal points, whereas the hollow circles are associated with orthogonal projections. Accordingly,

$$\begin{aligned} \xi_a^{(1)} &= \frac{2(\mathbf{q}_2^{(1)} - \mathbf{q}_1^{(1)}) \cdot (\mathbf{q}_1^{(2)} - \mathbf{q}_1^{(1)})}{\|\mathbf{q}_2^{(1)} - \mathbf{q}_1^{(1)}\|^2} - 1, & \xi_b^{(1)} &= 1 \\ \xi_b^{(2)} &= \frac{(2\mathbf{q}_2^{(1)} - \mathbf{q}_1^{(2)} - \mathbf{q}_2^{(2)}) \cdot (\mathbf{q}_2^{(1)} - \mathbf{q}_1^{(1)})}{(\mathbf{q}_2^{(2)} - \mathbf{q}_1^{(2)}) \cdot (\mathbf{q}_2^{(1)} - \mathbf{q}_1^{(1)})}, & \xi_a^{(2)} &= -1 \end{aligned} \tag{60}$$

Upon introduction of the three quadratic invariants

$$\begin{aligned} \pi_1(\mathbf{q}_{\text{seg}}) &= (\mathbf{q}_2^{(1)} - \mathbf{q}_1^{(1)}) \cdot (\mathbf{q}_2^{(1)} - \mathbf{q}_1^{(1)}) \\ \pi_2(\mathbf{q}_{\text{seg}}) &= (\mathbf{q}_2^{(1)} - \mathbf{q}_1^{(1)}) \cdot (\mathbf{q}_1^{(2)} - \mathbf{q}_1^{(1)}) \\ \pi_3(\mathbf{q}_{\text{seg}}) &= (\mathbf{q}_2^{(1)} - \mathbf{q}_1^{(1)}) \cdot (\mathbf{q}_2^{(2)} - \mathbf{q}_1^{(1)}) \end{aligned} \tag{61}$$

the quantities in (60) may be recast in the form

$$\begin{aligned} \tilde{\zeta}_a^{(1)} &= \frac{2\pi_2}{\pi_1} - 1, \quad \tilde{\zeta}_b^{(1)} = 1 \\ \tilde{\zeta}_b^{(2)} &= \frac{2\pi_1 - \pi_3 - \pi_2}{\pi_3 - \pi_2}, \quad \tilde{\zeta}_a^{(2)} = -1 \end{aligned} \tag{62}$$

Accordingly, (38) can be alternatively written as

$$\tilde{\zeta}^{(i)} = \frac{1}{2}(1 - \eta)\tilde{\zeta}_a^{(i)} + \frac{1}{2}(1 + \eta)\tilde{\zeta}_b^{(i)} \tag{63}$$

For the sake of completeness, we recast the formulation of $\tilde{\zeta}_b^{(1)}$ and $\tilde{\zeta}_a^{(2)}$, presuming that they are also associated with orthogonal projections

$$\begin{aligned} \tilde{\zeta}_b^{(1)} &= \frac{2(\mathbf{q}_2^{(1)} - \mathbf{q}_1^{(1)}) \cdot (\mathbf{q}_2^{(2)} - \mathbf{q}_1^{(1)})}{\|\mathbf{q}_2^{(1)} - \mathbf{q}_1^{(1)}\|^2} - 1 \\ \tilde{\zeta}_a^{(2)} &= \frac{(2\mathbf{q}_1^{(1)} - \mathbf{q}_1^{(2)} - \mathbf{q}_2^{(2)}) \cdot (\mathbf{q}_2^{(1)} - \mathbf{q}_1^{(1)})}{(\mathbf{q}_2^{(2)} - \mathbf{q}_1^{(2)}) \cdot (\mathbf{q}_2^{(1)} - \mathbf{q}_1^{(1)})} \end{aligned} \tag{64}$$

Employing the invariants (61) yields

$$\tilde{\zeta}_b^{(1)} = \frac{2\pi_3}{\pi_1} - 1 \quad \text{and} \quad \tilde{\zeta}_a^{(2)} = \frac{-\pi_3 - \pi_2}{\pi_3 - \pi_2} \tag{65}$$

Now, for $\alpha = 1$, the segment contribution (42) is given by

$$\Phi_{\text{seg}}^1 = \mathbf{v}_e \cdot \{n_{\text{seg}}^{11,(1)} \mathbf{q}_1^{(1)} + n_{\text{seg}}^{12,(1)} \mathbf{q}_2^{(1)} - (n_{\text{seg}}^{11,(2)} \mathbf{q}_1^{(2)} + n_{\text{seg}}^{12,(2)} \mathbf{q}_2^{(2)})\} \tag{66}$$

Making use of (43) together with (40) and (63), the last equation yields

$$\begin{aligned} \Phi_{\text{seg}}^1(\mathbf{q}_{\text{seg}}) &= \frac{1}{4} \mathbf{v}_e \cdot \left\{ (\mathbf{q}_1^{(1)} + \mathbf{q}_2^{(1)} - \mathbf{q}_1^{(2)} - \mathbf{q}_2^{(2)}) \int_{\gamma_c^{\text{seg}}} d\gamma \right. \\ &\quad + (-2\mathbf{q}_1^{(1)} + \mathbf{q}_1^{(2)} + \mathbf{q}_2^{(2)}) \int_{\gamma_c^{\text{seg}}} \tilde{\zeta}^{(1)} d\gamma + (\mathbf{q}_1^{(2)} - \mathbf{q}_2^{(2)}) \int_{\gamma_c^{\text{seg}}} \tilde{\zeta}^{(2)} d\gamma \\ &\quad \left. - (\mathbf{q}_1^{(2)} - \mathbf{q}_2^{(2)}) \int_{\gamma_c^{\text{seg}}} \tilde{\zeta}^{(1)} \tilde{\zeta}^{(2)} d\gamma - (\mathbf{q}_2^{(1)} - \mathbf{q}_1^{(1)}) \int_{\gamma_c^{\text{seg}}} (\tilde{\zeta}^{(1)})^2 d\gamma \right\} \end{aligned} \tag{67}$$

In the present case, the tangent vector

$$\frac{\partial \Phi^{(1)h}}{\partial \eta} = \frac{1}{4}(\mathbf{q}_2^{(1)} - \mathbf{q}_1^{(1)})(\tilde{\zeta}_b^{(1)} - \tilde{\zeta}_a^{(1)}) \tag{68}$$

does not depend on η . In this connection, use has been made of (39)₂, (40) and (63). Accordingly, the unit normal vector \mathbf{v}_e can be written as

$$\mathbf{v}_e = -\Lambda(\mathbf{q}_2^{(1)} - \mathbf{q}_1^{(1)}) / \|\mathbf{q}_2^{(1)} - \mathbf{q}_1^{(1)}\| \tag{69}$$

with the constant matrix

$$\Lambda = \begin{bmatrix} 0 & 1 \\ -1 & 0 \end{bmatrix} \tag{70}$$

Note that $\Lambda^T = \Lambda^{-1} = -\Lambda$ and $\Lambda^2 = -\mathbf{I}_2$. Let two additional quadratic invariants be defined as

$$\begin{aligned} \pi_4(\mathbf{q}_{\text{seg}}) &= (\mathbf{q}_2^{(1)} - \mathbf{q}_1^{(1)}) \cdot \Lambda(-2\mathbf{q}_1^{(1)} + \mathbf{q}_1^{(2)} + \mathbf{q}_2^{(2)}) \\ \pi_5(\mathbf{q}_{\text{seg}}) &= (\mathbf{q}_2^{(1)} - \mathbf{q}_1^{(1)}) \cdot \Lambda(\mathbf{q}_1^{(2)} - \mathbf{q}_2^{(2)}) \end{aligned} \tag{71}$$

Employing the invariants (61) and (71), and taking into account the skew-symmetry of Λ as well as the relationship

$$dy = \frac{1}{4} \|\mathbf{q}_2^{(1)} - \mathbf{q}_1^{(1)}\| (\tilde{\zeta}_b^{(1)} - \tilde{\zeta}_a^{(1)}) d\eta \tag{72}$$

which is consistent with (68), a straightforward calculation shows that constraint function (67) can be recast as

$$\tilde{\Phi}_{\text{seg}}^1(\boldsymbol{\pi}(\mathbf{q}_{\text{seg}})) = \frac{1}{16} (\tilde{\zeta}_b^{(1)} - \tilde{\zeta}_a^{(1)}) \left\{ \pi_4 \int_{-1}^1 (\tilde{\zeta}^{(1)} - 1) d\eta + \pi_5 \int_{-1}^1 (\tilde{\zeta}^{(2)} - \tilde{\zeta}^{(1)} \tilde{\zeta}^{(2)}) d\eta \right\} \tag{73}$$

Note that, with regard to (62) and (63), the evaluation of the integrals in (73) can be easily accomplished. For $\alpha=2$, the segment contribution (42) can be calculated along the same lines as before for $\alpha=1$ and yields

$$\tilde{\Phi}_{\text{seg}}^2(\boldsymbol{\pi}(\mathbf{q}_{\text{seg}})) = \frac{1}{16} (\tilde{\zeta}_b^{(1)} - \tilde{\zeta}_a^{(1)}) \left\{ \pi_5 \int_{-1}^1 (\tilde{\zeta}^{(2)} + \tilde{\zeta}^{(1)} \tilde{\zeta}^{(2)}) d\eta - \pi_4 \int_{-1}^1 (\tilde{\zeta}^{(1)} + 1) d\eta \right\} \tag{74}$$

It is easy to see that the invariants in (61) depend on \mathbb{S} . Moreover, since $\mathbf{a} \cdot \Lambda \mathbf{b} = \det([\mathbf{a}, \mathbf{b}])$ for any $\mathbf{a}, \mathbf{b} \in \mathbb{R}^2$, the invariants in (71) depend on \mathbb{T} . Accordingly, rotational invariance is satisfied by design. Furthermore, the proposed invariants π_i ($i = 1, \dots, 5$) fulfill condition (58) as well, which guarantees translational invariance.

In summary, the present reparametrization of the original mortar contact constraints (42) relies on a total of $d=5$ quadratic invariants specified in (61) and (71). Specifically, with regard to (58), (73), and (74) we get the final result

$$\tilde{\Phi}_{\text{seg}}^\alpha(\boldsymbol{\pi}(\mathbf{q}_{\text{seg}})) = \frac{1}{8} (\tilde{\zeta}_b^{(1)} - \tilde{\zeta}_a^{(1)}) \left\{ \pi_5 \int_{-1}^1 \tilde{\zeta}^{(2)} N^\alpha(\tilde{\zeta}^{(1)}) d\eta - \pi_4 \int_{-1}^1 N^\alpha(\tilde{\zeta}^{(1)}) d\eta \right\} \tag{75}$$

($\alpha = 1, 2$), where use has been made of the shape functions (40).

It is worth mentioning that the present reparametrization of the mortar contact constraints turned out to be beneficial to the computer implementation. In particular, the linearization of the mortar contact constraints in terms of the invariants has proven to be more manageable than the original version. Similar observations have been made within the framework of the NTS method, see Betsch and Hesch [3]. We refer to Appendix A for an outline of the linearization procedure.

3.3.4. Karush–Kuhn–Tucker conditions. According to the above exposition, the mortar contact constraints are associated with non-mortar nodes $A \in \bar{\omega}^{(1)}$. Specifically, the mortar contact constraints Φ^A follow from the assembly of the element contributions

$$\Phi_e^\alpha = \bigcup_{\text{seg}} \tilde{\Phi}_{\text{seg}}^\alpha(\boldsymbol{\pi}(\mathbf{q}_{\text{seg}})), \quad A = \text{LM}(\alpha, e) \quad (76)$$

as described in Sections 3.2 and 3.3. In the discrete contact problem the Karush–Kuhn–Tucker (KKT) conditions

$$\Phi^A \leq 0; \quad \lambda_A \geq 0; \quad \lambda_A \Phi^A = 0 \quad (77)$$

have to be satisfied. These conditions separate the set of potential contact nodes $\bar{\omega}^{(1)}$ into an active set \mathcal{A} and an inactive set \mathcal{I} , such that $\bar{\omega}^{(1)} = \mathcal{A} \cup \mathcal{I}$ and $\mathcal{A} \cap \mathcal{I} = \emptyset$.

4. DISCRETIZATION IN TIME

The equations of motion pertaining to the semi-discrete two-body system under consideration can be written as

$$\begin{aligned} \dot{\mathbf{q}} &= \mathbf{v} \\ \mathbf{M}\dot{\mathbf{v}} &= -\nabla V(\mathbf{q}) + \sum_{A \in \bar{\omega}^{(1)}} \lambda_A \nabla \Phi^A(\mathbf{q}) \end{aligned} \quad (78)$$

supplemented with the KKT conditions (77). For the purpose of time integration, we treat the equations of motion as differential-algebraic equations (DAEs). In this connection, the active set of contact constraints \mathcal{A} has to be consistent with the KKT conditions (see Section 4.3 for further details). Concerning the time discretization of the DAEs we apply a specific energy-momentum scheme, the design of which has been outlined in Betsch and Hesch [3, Section 3]. Accordingly, we arrive at the following one-step method:

$$\begin{aligned} \mathbf{q}_{n+1} - \mathbf{q}_n &= \frac{\Delta t}{2} (\mathbf{v}_n + \mathbf{v}_{n+1}) \\ \mathbf{M}(\mathbf{v}_{n+1} - \mathbf{v}_n) &= -\Delta t \bar{\nabla} V(\mathbf{q}_n, \mathbf{q}_{n+1}) - \Delta t \sum_{A \in \mathcal{A}} \lambda_{A,n+1} \bar{\nabla} \Phi^A(\mathbf{q}_n, \mathbf{q}_{n+1}) \\ 0 &= \Phi^A(\mathbf{q}_{n+1}), \quad A \in \mathcal{A} \end{aligned} \quad (79)$$

Here, $(\bullet)_n$ and $(\bullet)_{n+1}$ denote the approximations of the corresponding function at time t_n and t_{n+1} , respectively, $\Delta t = t_{n+1} - t_n$ is the time-step, and $\bar{\nabla}$ stands for a discrete gradient. Specifically,

the discrete gradient of the constraint function $\Phi^A(\mathbf{q})$ follows from the assembly of the element contributions

$$\bar{\nabla} \Phi_e^\alpha = \bigcup_{\text{seg}} D\boldsymbol{\pi}(\mathbf{q}_{\text{seg},n+\frac{1}{2}})^T \bar{\bar{\nabla}} \tilde{\Phi}_{\text{seg}}^\alpha(\boldsymbol{\pi}(\mathbf{q}_{\text{seg},n}), \boldsymbol{\pi}(\mathbf{q}_{\text{seg},n+1})) \tag{80}$$

for $A = \text{LM}(\alpha, e)$, where

$$\bar{\bar{\nabla}} \tilde{\Phi}_{\text{seg}}^\alpha(\boldsymbol{\pi}_n, \boldsymbol{\pi}_{n+1}) = \nabla \tilde{\Phi}_{\text{seg}}^\alpha(\boldsymbol{\pi}_{n+\frac{1}{2}}) + \frac{\tilde{\Phi}_{\text{seg}}^\alpha(\boldsymbol{\pi}_{n+1}) - \tilde{\Phi}_{\text{seg}}^\alpha(\boldsymbol{\pi}_n) - \nabla \tilde{\Phi}_{\text{seg}}^\alpha(\boldsymbol{\pi}_{n+\frac{1}{2}}) \cdot \Delta\boldsymbol{\pi}}{\|\Delta\boldsymbol{\pi}\|^2} \Delta\boldsymbol{\pi} \tag{81}$$

In this connection, the abbreviations $\boldsymbol{\pi}_n = \boldsymbol{\pi}(\mathbf{q}_{\text{seg},n})$, $\boldsymbol{\pi}_{n+1} = \boldsymbol{\pi}(\mathbf{q}_{\text{seg},n+1})$, $\Delta\boldsymbol{\pi} = \boldsymbol{\pi}_{n+1} - \boldsymbol{\pi}_n$, and $(\bullet)_{n+\frac{1}{2}} = ((\bullet)_n + (\bullet)_{n+1})/2$ have been employed.

4.1. Algorithmic conservation of momentum maps

The application of the discrete gradient (80) in the calculation of the algorithmic constraint forces enables conservation of the linear and angular momentum. In essence, these conservation properties are due to the use of the quadratic invariants in (80). Specifically, in complete analogy to the time-continuous case dealt with in Section 3.3, the following relationships are satisfied in the fully discrete setting:

$$D\Phi_{\text{seg}}(\mathbf{q}_{\text{seg},n+\frac{1}{2}}) \begin{bmatrix} \xi \\ \xi \\ \xi \\ \xi \end{bmatrix} = \mathbf{0} \tag{82}$$

and

$$D\Phi_{\text{seg}}(\mathbf{q}_{\text{seg},n+\frac{1}{2}}) \begin{bmatrix} \xi \times \mathbf{q}_{1,n+\frac{1}{2}}^{(1)} \\ \xi \times \mathbf{q}_{2,n+\frac{1}{2}}^{(1)} \\ \xi \times \mathbf{q}_{1,n+\frac{1}{2}}^{(2)} \\ \xi \times \mathbf{q}_{2,n+\frac{1}{2}}^{(2)} \end{bmatrix} = \mathbf{0} \tag{83}$$

Equation (82) can be regarded as a discrete counterpart of (53), and allows algorithmic conservation of the total linear momentum. Similarly, Equation (83) can be viewed as a discrete counterpart of (55), and enables algorithmic conservation of the total angular momentum.

4.2. Conservation of energy

For frictionless contact problems the net contact power input to the system is zero (see Laursen [4, Section 7.2.1]). This feature allows conservation of the system’s total energy.

Assume that $\delta\boldsymbol{\varphi}^{(i)} = \dot{\boldsymbol{\varphi}}^{(i)}$ are feasible variations (cf. Section 3.3). Substituting $\delta\boldsymbol{\varphi}^{(i)} = \dot{\boldsymbol{\varphi}}^{(i)}$ into expression (12) for the continuous representation of the contact virtual work yields the total power

input of the contact stresses

$$\mathcal{P}^{\text{con}} := \sum_{i=1}^2 G^{(i),c}(\boldsymbol{\varphi}^{(i)}, \dot{\boldsymbol{\varphi}}^{(i)}) \tag{84}$$

Conservation of energy implies $\mathcal{P}^{\text{con}}=0$. Similarly, for the semi-discrete system, substituting $\delta\mathbf{q}=\dot{\mathbf{q}}$ into (45) yields

$$\begin{aligned} \mathcal{P}^{\text{con,h}} &= \dot{\mathbf{q}} \cdot \left\{ \sum_{A \in \bar{\omega}^{(1)}} \lambda_A \nabla \Phi^A(\mathbf{q}) \right\} \\ &= \sum_{A \in \bar{\omega}^{(1)}} \lambda_A \dot{\Phi}^A \end{aligned} \tag{85}$$

Consequently, $\mathcal{P}^{\text{con,h}}=0$, if the space-discrete persistency condition $\lambda_A \dot{\Phi}^A=0$ is satisfied for $A \in \bar{\omega}^{(1)}$. Note that, with regard to (46), $\mathcal{P}^{\text{con,h}}$ can also be written in the form

$$\mathcal{P}^{\text{con,h}} = \sum_{e \in \bar{e}^{(1)}} \left(\bigcup_{\text{seg}} \dot{\mathbf{q}}_{\text{seg}} \cdot D\boldsymbol{\Phi}_{\text{seg}}^T(\mathbf{q}_{\text{seg}}) \right) \lambda^e \tag{86}$$

4.2.1. *Algorithmic conservation of energy.* In the fully discrete setting algorithmic energy conservation is facilitated by the use of the discrete gradient (80), provided that a discrete version of the aforementioned persistency condition holds. Specifically, the discrete counterpart of $\mathcal{P}^{\text{con,h}}$ can be written as

$$\begin{aligned} \tilde{\mathcal{P}}^{\text{con,h}} &= \frac{1}{\Delta t} \sum_{A \in \mathcal{A}} \lambda_{A,n+1} \bar{\nabla} \Phi^A(\mathbf{q}_n, \mathbf{q}_{n+1}) \cdot (\mathbf{q}_{n+1} - \mathbf{q}_n) \\ &= \frac{1}{\Delta t} \sum_{A \in \mathcal{A}} \lambda_{A,n+1} (\Phi^A(\mathbf{q}_{n+1}) - \Phi^A(\mathbf{q}_n)) \end{aligned} \tag{87}$$

The last equality holds since, with regard to (86), (80), and (81),

$$\begin{aligned} &(\mathbf{q}_{\text{seg},n+1} - \mathbf{q}_{\text{seg},n}) \cdot D\boldsymbol{\pi}(\mathbf{q}_{\text{seg},n+\frac{1}{2}})^T \bar{\nabla} \tilde{\Phi}_{\text{seg}}^\alpha(\boldsymbol{\pi}_n, \boldsymbol{\pi}_{n+1}) \\ &= (\boldsymbol{\pi}_{n+1} - \boldsymbol{\pi}_n) \cdot \bar{\nabla} \tilde{\Phi}_{\text{seg}}^\alpha(\boldsymbol{\pi}_n, \boldsymbol{\pi}_{n+1}) = \tilde{\Phi}_{\text{seg}}^\alpha(\boldsymbol{\pi}_{n+1}) - \tilde{\Phi}_{\text{seg}}^\alpha(\boldsymbol{\pi}_n) \end{aligned} \tag{88}$$

and, since both $\Phi^A(\mathbf{q}_{n+1})$ and $\Phi^A(\mathbf{q}_n)$ result from the assembly of the element contributions

$$\Phi_{e,n+1}^\alpha = \bigcup_{\text{seg}} \tilde{\Phi}_{\text{seg}}^\alpha(\boldsymbol{\pi}_{n+1}) \quad \text{and} \quad \Phi_{e,n}^\alpha = \bigcup_{\text{seg}} \tilde{\Phi}_{\text{seg}}^\alpha(\boldsymbol{\pi}_n) \tag{89}$$

for $A=\text{LM}(\alpha, e)$. Accordingly, algorithmic conservation of energy is facilitated if the discrete persistency condition

$$\lambda_{A,n+1} (\Phi^A(\mathbf{q}_{n+1}) - \Phi^A(\mathbf{q}_n)) = 0 \tag{90}$$

is fulfilled.

Note, however, that the discrete persistency condition is not satisfied in general. For example, in the case of impact problems, the active set \mathcal{A} generally changes from t_n to t_{n+1} . Therefore,

a previously inactive constraint Φ^A may be detected active at t_{n+1} . In general, this constraint is not satisfied at t_n and thus the discrete consistency condition is violated. In the event of such an inconsistency we replace the original constraint function in (79)₃ according to

$$\Phi^A(\mathbf{q}_{n+1}) \rightarrow \bar{\Phi}^A(\mathbf{q}_{n+1}) - \Phi^A(\mathbf{q}_n) \tag{91}$$

so that condition (90) is still satisfied. This approach can be viewed as modification of the configuration manifold specified by the active contact constraints. It is worth noting that the present modification for maintaining algorithmic energy conservation does not affect algorithmic conservation of the linear and angular momentum.

Concerning the application of the discrete gradient to the potential energy function in (79)₂ we choose

$$\bar{\nabla} V(\mathbf{q}_n, \mathbf{q}_{n+1}) = \bar{\nabla} V^{\text{int}}(\mathbf{q}_n, \mathbf{q}_{n+1}) + \nabla V^{\text{ext}}(\mathbf{q}_{n+\frac{1}{2}}) \tag{92}$$

where use has been made of (27). Here, $\bar{\nabla} V^{\text{int}}$ stands for the application of a discrete gradient to the stored energy function. In this connection, the components of the discrete deformation tensor play the role of quadratic invariants (see Betsch and Hesch [3, Section 3.4]). For St. Venant–Kirchhoff material this approach boils down to the use of an averaged strain tensor as originally proposed by Simo and Tarnow [27], see also Laursen [4, Remark 7.2].

4.3. Implementation

We next deal with the numerical implementation of the algebraic problem emanating from the scheme (79). To account for the contact conditions we make use of an active set strategy proposed by Hüeber and Wohlmuth [8], see also Hartmann *et al.* [12] and the references cited in these works. Substituting for \mathbf{v}_{n+1} from (79)₁ into (79)₂, yields the non-linear system of equations

$$\mathbf{R}(\mathbf{q}_{n+1}, [\lambda_{A,n+1}]) := \begin{bmatrix} \mathbf{R}_q \\ [\Phi^A] \end{bmatrix} = \mathbf{0}, \quad A \in \mathcal{A} \tag{93}$$

where

$$\mathbf{R}_q = \frac{2}{\Delta t} \mathbf{M}(\mathbf{q}_{n+1} - \mathbf{q}_n) - 2\mathbf{M}\mathbf{v}_n + \Delta t \bar{\nabla} V(\mathbf{q}_n, \mathbf{q}_{n+1}) + \Delta t \sum_{A \in \mathcal{A}} \lambda_{A,n+1} \bar{\nabla} \Phi^A(\mathbf{q}_n, \mathbf{q}_{n+1}) \tag{94}$$

Once the system (93) has been solved for \mathbf{q}_{n+1} and $\lambda_{A,n+1}$, $A \in \mathcal{A}$, the unknown velocities can be computed via

$$\mathbf{v}_{n+1} = \frac{2}{\Delta t} (\mathbf{q}_{n+1} - \mathbf{q}_n) - \mathbf{v}_n \tag{95}$$

The solution of the non-linear system of equations (93) is embedded into an active set algorithm that can be summarized as follows:

- (1) Choose an initial subdivision of the set of potential contact constraints $\bar{\omega}^{(1)}$ into an active set \mathcal{A}_1 and an inactive set \mathcal{I}_1 , such that $\bar{\omega}^{(1)} = \mathcal{A}_1 \cup \mathcal{I}_1$ and $\mathcal{A}_1 \cap \mathcal{I}_1 = \emptyset$, and set $k = 1$.
- (2) Solve the non-linear system of equations (93) for \mathbf{q}_{n+1} and $\lambda_{A,n+1}$ for $A \in \mathcal{A}_k$; $\lambda_{A,n+1} = 0$ for $A \in \mathcal{I}_k$.

(3) Update the sets \mathcal{A}_k and \mathcal{I}_k according to

$$\mathcal{A}_{k+1} = \{A \in \bar{\omega}^{(1)} : \lambda_{A,n+1} + c\Phi^A(\mathbf{q}_{n+1}) > 0\}$$

$$\mathcal{I}_{k+1} = \{A \in \bar{\omega}^{(1)} : \lambda_{A,n+1} + c\Phi^A(\mathbf{q}_{n+1}) \leq 0\}$$

(for some $c > 0$), and repeat the procedure with new iteration counter $k+1$ until the sets remain unchanged.

To solve the non-linear system in step (2) we apply Newton's method. The linearization of (93) leads to the following generalized saddle point system that has to be solved in each Newton iteration:

$$\begin{bmatrix} \mathcal{N} & \tilde{\mathcal{G}}^T \\ \mathcal{G} & \mathbf{0} \end{bmatrix} \begin{bmatrix} \Delta \mathbf{q} \\ \Delta \tilde{\lambda} \end{bmatrix} = - \begin{bmatrix} \mathbf{R}_q \\ \mathbf{R}_\lambda \end{bmatrix} \quad (96)$$

where

$$\mathcal{N} = D_1 \mathbf{R}_q(\mathbf{q}_{n+1}, \lambda_{n+1}), \quad \mathcal{G} = D\Phi(\mathbf{q}_{n+1}), \quad \tilde{\mathcal{G}} = D_2 \mathbf{R}_q(\mathbf{q}_{n+1}, \lambda_{n+1})^T$$

$$\mathbf{R}_\lambda = \Phi(\mathbf{q}_{n+1}), \quad \Delta \tilde{\lambda} = \Delta t \Delta \lambda$$

Although the above saddle point system could be directly solved, we advocate a reformulation of (96), which fits into the framework of the discrete null space method.

5. DISCRETE NULL SPACE METHOD

The direct discretization of the DAEs governing the motion of constrained mechanical systems necessitates the solution of saddle point systems of the form (96). In this context, the discrete null space method has been developed by the second author [28] to achieve a size-reduction along with an improved conditioning of the system to be solved. Our approach can be linked to null space methods often used in optimization, cf. Benzi *et al.* [29, Section 6].

Let n be the number of redundant coordinates and m be the number of constraints. We start with the introduction of a change of coordinates

$$\Delta \mathbf{q} = \mathbf{U} \Delta \mathbf{u} \quad (97)$$

with $\Delta \mathbf{u} \in \mathbb{R}^n$ and a non-singular transformation matrix $\mathbf{U} \in \mathbb{R}^{n \times n}$. Next, split $\Delta \mathbf{u}$ into independent coordinates $\Delta \mathbf{u}_I \in \mathbb{R}^{n-m}$ and dependent coordinates $\Delta \mathbf{u}_D \in \mathbb{R}^m$, such that

$$\Delta \mathbf{u} = \begin{bmatrix} \Delta \mathbf{u}_I \\ \Delta \mathbf{u}_D \end{bmatrix} \quad (98)$$

and, correspondingly, $\mathbf{U} = [\mathbf{U}_I, \mathbf{U}_D]$. In this connection, we require that the $m \times m$ matrix $\tilde{\mathcal{G}} \mathbf{U}_D$ is invertible. Making use of the above coordinate partitioning, (97) can be recast in the form

$$\Delta \mathbf{q} = \mathbf{U}_I \Delta \mathbf{u}_I + \mathbf{U}_D \Delta \mathbf{u}_D \quad (99)$$

Premultiplying the first row in (96) by \mathbf{U}^T yields

$$\mathbf{U}_I^T \mathcal{N} \Delta \mathbf{q} + \mathbf{U}_I^T \tilde{\mathcal{G}}^T \Delta \tilde{\lambda} = -\mathbf{U}_I^T \mathbf{R}_q \tag{100}$$

$$\mathbf{U}_D^T \mathcal{N} \Delta \mathbf{q} + \mathbf{U}_D^T \tilde{\mathcal{G}}^T \Delta \tilde{\lambda} = -\mathbf{U}_D^T \mathbf{R}_q \tag{101}$$

The second of the above equations gives rise to

$$\Delta \tilde{\lambda} = -(\tilde{\mathcal{G}} \mathbf{U}_D)^{-T} \mathbf{U}_D^T [\mathbf{R}_q + \mathcal{N} \Delta \mathbf{q}] \tag{102}$$

Substituting the last equation into (100) leads to

$$\tilde{\mathbf{P}}^T \mathcal{N} \Delta \mathbf{q} = -\tilde{\mathbf{P}}^T \mathbf{R}_q \tag{103}$$

where the $n \times (n - m)$ matrix

$$\tilde{\mathbf{P}} := (\mathbf{I}_n - \mathbf{U}_D (\tilde{\mathcal{G}} \mathbf{U}_D)^{-1} \tilde{\mathcal{G}}) \mathbf{U}_I \tag{104}$$

can be identified as a discrete null space matrix (cf. Betsch [28, Section 3.2.1]). Note that, by design, $\tilde{\mathbf{P}}$ spans the null space of the discrete constraint Jacobian $\tilde{\mathcal{G}}$. Consequently, $\tilde{\mathcal{G}} \tilde{\mathbf{P}} = \mathbf{0}$. Now the generalized saddle point system (96) can be solved by applying two successive steps. First solve

$$\begin{bmatrix} \tilde{\mathbf{P}}^T \mathcal{N} \\ \tilde{\mathcal{G}} \end{bmatrix} \Delta \mathbf{q} = - \begin{bmatrix} \tilde{\mathbf{P}}^T \mathbf{R}_q \\ \mathbf{R}_\lambda \end{bmatrix} \tag{105}$$

for $\Delta \mathbf{q} \in \mathbb{R}^n$. Then (102) can be used to determine $\Delta \lambda \in \mathbb{R}^m$. Table I contains a summary of the solution procedure, which is embedded into the active set strategy as outlined in Section 4.3.

5.1. Alternative solution of the reduced system

We next outline a further reformulation of the system to be solved that retains the symmetry in case the underlying saddle point system (96) is symmetric, e.g. for equilibrium problems. The size-reduced system (105) may be solved alternatively by making use of the generalized coordinate partitioning (99) again. To this end, the second row in (105) may be written as

$$\mathcal{G} \mathbf{U}_I \Delta \mathbf{u}_I + \mathcal{G} \mathbf{U}_D \Delta \mathbf{u}_D = -\mathbf{R}_\lambda \tag{106}$$

so that

$$\Delta \mathbf{u}_D = -(\mathcal{G} \mathbf{U}_D)^{-1} [\mathbf{R}_\lambda + \mathcal{G} \mathbf{U}_I \Delta \mathbf{u}_I] \tag{107}$$

Now the first row in (105), in conjunction with (99) and (107), can be recast in the form

$$\tilde{\mathbf{P}}^T \mathcal{N} \mathbf{P} \Delta \mathbf{u}_I = -\tilde{\mathbf{P}}^T [\mathbf{R}_q - \mathcal{N} \mathbf{U}_D (\mathcal{G} \mathbf{U}_D)^{-1} \mathbf{R}_\lambda] \tag{108}$$

where

$$\mathbf{P} := (\mathbf{I}_n - \mathbf{U}_D (\mathcal{G} \mathbf{U}_D)^{-1} \mathcal{G}) \mathbf{U}_I \tag{109}$$

Table I. Solution procedure for one representative time-step.

-
- (1) Subdivide the set of all possible contact constraints $\bar{\omega}^{(1)}$ into the set of active constraints \mathcal{A}_k and the set of inactive constraints \mathcal{I}_k , such that $\bar{\omega}^{(1)} = \mathcal{A}_k \cup \mathcal{I}_k$ and $\mathcal{A}_k \cap \mathcal{I}_k = \emptyset$, and set $k=1$ for initialization.
- (2) Find $\mathbf{q}_{n+1} \in \mathbb{R}^n$ and $\lambda_{A,n+1} = [\lambda_{A,n+1}]$ for $A \in \mathcal{A}_k$ ($\lambda_{A,n+1} = 0$ for $A \in \mathcal{I}_k$), set the iteration index $l=1$.

- (2.1) Given $\mathbf{q}_{n+1}^{(l)}$ and $\lambda_{n+1}^{(l)}$, calculate the residual vector

$$\mathbf{R}^{(l)} = \begin{bmatrix} \mathbf{R}_q(\mathbf{q}_{n+1}^{(l)}, \lambda_{n+1}^{(l)}) \\ \mathbf{R}_\lambda(\mathbf{q}_{n+1}^{(l)}) \end{bmatrix}$$

and check for convergence, i.e. check whether $\|\mathbf{R}^{(l)}\| < \varepsilon$, where ε is a prescribed tolerance.

- (2.2) If convergence has not been attained, calculate the discrete null space matrix

$$\tilde{\mathbf{P}}^{(l)} = (\mathbf{I}_n - \mathbf{U}_D^{(l)} (\tilde{\mathcal{G}}^{(l)} \mathbf{U}_D^{(l)})^{-1} \tilde{\mathcal{G}}^{(l)}) \mathbf{U}_I^{(l)}$$

and solve the algebraic system of linear equations

$$\begin{bmatrix} \tilde{\mathbf{P}}^{(l)\text{T}} \mathcal{N}^{(l)} \\ \tilde{\mathcal{G}}^{(l)} \end{bmatrix} \Delta \mathbf{q} = - \begin{bmatrix} \tilde{\mathbf{P}}^{(l)\text{T}} \mathbf{R}_q^{(l)} \\ \mathbf{R}_\lambda^{(l)} \end{bmatrix}$$

Now, determine $\Delta \lambda$ via

$$\Delta \lambda = - \frac{1}{\Delta t} (\tilde{\mathcal{G}}^{(l)} \mathbf{U}_D^{(l)})^{-\text{T}} \mathbf{U}_D^{(l)\text{T}} [\mathbf{R}_q^{(l)} + \mathcal{N}^{(l)} \Delta \mathbf{q}]$$

- (2.3) Update the unknowns according to

$$\mathbf{q}_{n+1}^{(l+1)} = \mathbf{q}_{n+1}^{(l)} + \Delta \mathbf{q}$$

$$\lambda_{n+1}^{(l+1)} = \lambda_{n+1}^{(l)} + \Delta \lambda$$

and repeat the procedure with new iteration counter $l+1$ until convergence.

- (3) Update the sets \mathcal{A}_k and \mathcal{I}_k according to

$$\mathcal{A}_{k+1} = \{A \in \bar{\omega}^{(1)} : \lambda_{A,n+1} + c \Phi_A(\mathbf{q}_{n+1}) > 0\}$$

$$\mathcal{I}_{k+1} = \{A \in \bar{\omega}^{(1)} : \lambda_{A,n+1} + c \Phi_A(\mathbf{q}_{n+1}) \leq 0\}$$

(for some $c > 0$), and repeat the procedure with new iteration counter $k+1$ until the sets remain unchanged.

The solution of (105) is given by

$$\Delta \mathbf{q} = \mathbf{U}_I \Delta \mathbf{u}_I + \mathbf{U}_D \Delta \mathbf{u}_D \tag{110}$$

where $\Delta \mathbf{u}_I \in \mathbb{R}^{n-m}$ can be obtained from (108) and $\Delta \mathbf{u}_D \in \mathbb{R}^m$ from (107). In essence, the implementation of this approach is contained in [28, Table 3]. It is worth noting that the staggered solution for $\Delta \mathbf{u}_I$ and $\Delta \mathbf{u}_D$ corresponds to the application of forward substitution to the block lower triangular system

$$\begin{bmatrix} \tilde{\mathbf{P}}^T \mathcal{A} \mathbf{P} & \mathbf{0} \\ \mathcal{G} \mathbf{U}_I & \mathcal{G} \mathbf{U}_D \end{bmatrix} \begin{bmatrix} \Delta \mathbf{u}_I \\ \Delta \mathbf{u}_D \end{bmatrix} = - \begin{bmatrix} \tilde{\mathbf{P}}^T \mathbf{R}_q \\ \mathbf{R}_\lambda \end{bmatrix} \tag{111}$$

Premultiplying Equation (111) by

$$\begin{bmatrix} \mathbf{I}_{n-m} & (\mathcal{G} \mathbf{U}_I)^T \\ \mathbf{0} & (\mathcal{G} \mathbf{U}_D)^T \end{bmatrix} \tag{112}$$

yields

$$\left\{ \begin{bmatrix} \tilde{\mathbf{P}}^T \mathcal{A} \mathbf{P} & \mathbf{0} \\ \mathbf{0} & \mathbf{0} \end{bmatrix} + (\tilde{\mathcal{G}} \mathbf{U})^T \mathcal{G} \mathbf{U} \right\} \begin{bmatrix} \Delta \mathbf{u}_I \\ \Delta \mathbf{u}_D \end{bmatrix} = - \begin{bmatrix} \tilde{\mathbf{P}}^T \mathbf{R}_q \\ \mathbf{0} \end{bmatrix} - (\tilde{\mathcal{G}} \mathbf{U})^T \mathbf{R}_\lambda \tag{113}$$

It can be easily verified by a straightforward calculation, that (113) can be written in the alternative form

$$\{\tilde{\mathbf{\Pi}}^T \mathbf{U}^T \mathcal{A} \mathbf{U} \mathbf{\Pi} + (\tilde{\mathcal{G}} \mathbf{U})^T \mathcal{G} \mathbf{U}\} \begin{bmatrix} \Delta \mathbf{u}_I \\ \Delta \mathbf{u}_D \end{bmatrix} = -\tilde{\mathbf{\Pi}}^T \mathbf{U}^T \mathbf{R}_q - (\tilde{\mathcal{G}} \mathbf{U})^T \mathbf{R}_\lambda \tag{114}$$

with

$$\tilde{\mathbf{\Pi}} := \mathbf{I}_n - \tilde{\mathbf{W}} \tilde{\mathcal{G}} \mathbf{U}, \quad \tilde{\mathbf{W}} = \begin{bmatrix} \mathbf{0}_{(n-m) \times m} \\ (\tilde{\mathcal{G}} \mathbf{U}_D)^{-1} \end{bmatrix} \tag{115}$$

and

$$\mathbf{\Pi} := \mathbf{I}_n - \mathbf{W} \mathcal{G} \mathbf{U}, \quad \mathbf{W} = \begin{bmatrix} \mathbf{0}_{(n-m) \times m} \\ (\mathcal{G} \mathbf{U}_D)^{-1} \end{bmatrix} \tag{116}$$

We finally remark that the described procedure for solving the underlying saddle point system (96) is closely related to previous works by Krause and Wohlmuth [30, Section 3] and Ainsworth [31] dealing with the solution of symmetric saddle point systems.

5.2. Application to contact problems

The application of the discrete null space method to the contact problems under consideration rests on the design of a viable discrete null space matrix (104). To this end, the matrices \mathbf{U}_I and \mathbf{U}_D resulting from a suitable coordinate partitioning of the form (98) have to be devised.

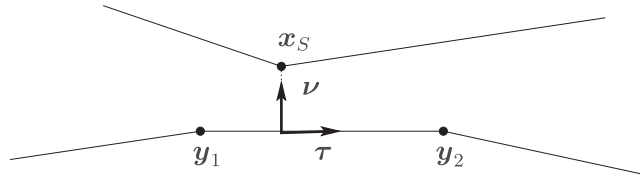


Figure 3. Node-to-segment contact element.

5.2.1. *NTS contact element.* We first illustrate our approach with the NTS method dealt with in Betsch and Hesch [3, Section 3.5]. Accordingly, consider a representative NTS contact element (Figure 3) with the vector of relevant nodal coordinates

$$\bar{\mathbf{q}} = \begin{bmatrix} \mathbf{x}_S \\ \mathbf{y}_1 \\ \mathbf{y}_2 \end{bmatrix} \tag{117}$$

Note that to each slave node \mathbf{x}_S , there is associated one constraint of impenetrability. We now perform the decomposition

$$\Delta \mathbf{x}_S = \tau \Delta u_{S,I} + \nu \Delta u_{S,D} \tag{118}$$

where, on the master side, the unit tangent and normal vectors are defined by

$$\begin{aligned} \boldsymbol{\tau} &= (\mathbf{y}_2 - \mathbf{y}_1) / \|\mathbf{y}_2 - \mathbf{y}_1\| \\ \boldsymbol{\nu} &= -\boldsymbol{\Lambda} \boldsymbol{\tau} \end{aligned} \tag{119}$$

and $\boldsymbol{\Lambda}$ is given by (70). According to (118), the displacement of the slave node $u_{S,D}$ in normal direction has been chosen as dependent coordinate. Now, for the NTS element under consideration, the partitioning (99) can be written as

$$\Delta \bar{\mathbf{q}} = \bar{\mathbf{U}}_I \Delta \bar{\mathbf{u}}_I + \bar{\mathbf{U}}_D \Delta \bar{u}_D \tag{120}$$

where

$$\Delta \bar{\mathbf{u}}_I = \begin{bmatrix} \Delta u_{S,I} \\ \Delta \mathbf{y}_1 \\ \Delta \mathbf{y}_2 \end{bmatrix}, \quad \Delta \bar{u}_D = \Delta u_{S,D} \tag{121}$$

and

$$\bar{\mathbf{U}}_I = \begin{bmatrix} \boldsymbol{\tau} & \mathbf{0} & \mathbf{0} \\ \mathbf{0} & \mathbf{I}_2 & \mathbf{0} \\ \mathbf{0} & \mathbf{0} & \mathbf{I}_2 \end{bmatrix}, \quad \bar{\mathbf{U}}_D = \begin{bmatrix} \boldsymbol{\nu} \\ \mathbf{0} \\ \mathbf{0} \end{bmatrix} \tag{122}$$

Since the constraint Jacobian pertaining to the NTS element is given by (cf. Betsch and Hesch [3, Equation (71)])

$$\bar{\mathcal{G}} = [\boldsymbol{\nu}^T \quad -N^1 \boldsymbol{\nu}^T \quad -N^2 \boldsymbol{\nu}^T] \tag{123}$$

we obtain

$$\overline{\mathcal{G}}\mathbf{U}_D = \mathbf{v} \cdot \mathbf{v} = 1 \tag{124}$$

Accordingly, in the static case, Equation (104) for the null space matrix (which is identical to (109) in the case of equilibrium problems) can be evaluated in a straightforward way, taking into account that, due to property (124), $\overline{\mathcal{G}}\mathbf{U}_D$ coincides with the $m \times m$ identity matrix. Thus, (104) gives the null space matrix

$$\mathbf{P} = (\mathbf{I}_n - \mathbf{U}_D \overline{\mathcal{G}})\mathbf{U}_I \tag{125}$$

where the $n \times m$ matrix \mathbf{U}_D follows from the assembly of the matrices $\overline{\mathbf{U}}_D$ pertaining to the respective slave node. The $n \times (n - m)$ matrix \mathbf{U}_I can be viewed as modification of the identity matrix resulting from the contributions $\overline{\mathbf{U}}_I$ of the slave nodes, given by (122). It is worth remarking that recently Muñoz [32] proposed an alternative way to set up a null space matrix for the NTS method based on a global parametrization of the master surface in terms of cubic B-splines. Yet another related approach can be found in Chow *et al.* [33].

For transient problems, in (104), $\overline{\mathcal{G}}$ contains the contributions of the discrete constraint gradient associated with each slave node, $\overline{\nabla}_{\overline{\mathbf{q}}} \Phi_S(\overline{\mathbf{q}}_n, \overline{\mathbf{q}}_{n+1})$ (cf. Betsch and Hesch [3, Equation (75)]). In this case we choose

$$\overline{\mathbf{U}}_I = \begin{bmatrix} \overline{\boldsymbol{\tau}} & \mathbf{0} & \mathbf{0} \\ \mathbf{0} & \mathbf{I}_2 & \mathbf{0} \\ \mathbf{0} & \mathbf{0} & \mathbf{I}_2 \end{bmatrix}, \quad \overline{\mathbf{U}}_D = \begin{bmatrix} \overline{\mathbf{v}} \\ \mathbf{0} \\ \mathbf{0} \end{bmatrix} \tag{126}$$

where

$$\overline{\mathbf{v}} = \boldsymbol{\zeta} / \|\boldsymbol{\zeta}\|, \quad \overline{\boldsymbol{\tau}} = \boldsymbol{\Lambda} \overline{\mathbf{v}}, \quad \boldsymbol{\zeta} = \overline{\nabla}_{\mathbf{x}_S} \Phi_S(\overline{\mathbf{q}}_n, \overline{\mathbf{q}}_{n+1}) \tag{127}$$

Similar to the static case, property (124) holds again. Consequently, analogous to (125), the discrete null space matrix assumes the form

$$\tilde{\mathbf{P}} = (\mathbf{I}_n - \mathbf{U}_D \tilde{\mathcal{G}})\mathbf{U}_I \tag{128}$$

where, as before, \mathbf{U}_I and \mathbf{U}_D are associated with the slave node contributions (126).

5.2.2. Mortar contact description. Guided by our previous developments in the context of the NTS method, we choose the nodes on the non-mortar side to perform a decomposition similar to (118). Accordingly, consider the position vector $\mathbf{q}_A^{(1)}$ on the non-mortar side (i.e. $A \in \overline{\omega}^{(1)}$) and perform the split

$$\Delta \mathbf{q}_A^{(1)} = \boldsymbol{\tau}_A^{(1)} \Delta u_{A,I}^{(1)} + \mathbf{v}_A^{(1)} \Delta u_{A,D}^{(1)} \tag{129}$$

where

$$\mathbf{v}_A = \boldsymbol{\zeta}_A / \|\boldsymbol{\zeta}_A\|, \quad \boldsymbol{\tau}_A = \boldsymbol{\Lambda} \mathbf{v}_A, \quad \boldsymbol{\zeta}_A = \overline{\nabla}_{\mathbf{q}_A^{(1)}} \Phi^A(\mathbf{q}_n, \mathbf{q}_{n+1}) \tag{130}$$

Taking into account the structure of the system configuration vector (16), the above decomposition gives rise to

$$\begin{bmatrix} \Delta \mathbf{q}_1^{(1)} \\ \vdots \\ \Delta \mathbf{q}_A^{(1)} \\ \vdots \\ \Delta \mathbf{q}^{(2)} \end{bmatrix} = \underbrace{\begin{bmatrix} \mathbf{I}_2 & & & \\ & \ddots & & \\ & & \boldsymbol{\tau}_A^{(1)} & \\ & & & \ddots \\ & & & & \mathbf{I}_{2n_{\text{node}}^{(2)}} \end{bmatrix}}_{\mathbf{U}_{I,A}} \begin{bmatrix} \Delta \mathbf{q}_1^{(1)} \\ \vdots \\ \Delta u_{A,I}^{(1)} \\ \vdots \\ \Delta \mathbf{q}^{(2)} \end{bmatrix} + \underbrace{\begin{bmatrix} \mathbf{0} \\ \vdots \\ \mathbf{v}_A^{(1)} \\ \vdots \\ \mathbf{0} \end{bmatrix}}_{\mathbf{U}_{D,A}} \Delta u_{A,D}^{(1)} \quad (131)$$

The assembly of the column matrices $\mathbf{U}_{D,A}$ yields the $n \times m$ matrix \mathbf{U}_D . Note that, by design, the diagonal elements of the $m \times m$ matrix $\mathcal{G}\mathbf{U}_D$ are equal to 1. However, in contrast to the NTS method treated above, $\mathcal{G}\mathbf{U}_D$ does not coincide with the identity matrix anymore. Due to the structure of the mortar contact constraints, $\mathcal{G}\mathbf{U}_D$ has at most three non-zero elements per row. With regard to (104), the discrete null space matrix is given by

$$\tilde{\mathbf{P}} = (\mathbf{I}_n - \mathbf{U}_D(\mathcal{G}\mathbf{U}_D)^{-1}\mathcal{G})\mathbf{U}_I \quad (132)$$

where \mathbf{U}_I is an $n \times (n - m)$ matrix, which results from the $n \times n$ identity matrix by replacing the 2×2 block identity matrices on the diagonal with column vectors $\boldsymbol{\tau}_A^{(1)}$ (cf. Equation (131)).

6. NUMERICAL EXAMPLES

6.1. Persistent contact problem

The first numerical example presented herein consists of the planar model of a bearing depicted in Figure 4. A similar example dealing with two concentric rings has been presented by Belytschko *et al.* [34] to investigate the performance of a specific smoothing algorithm.

The bearing consists of two rings (Young's modulus $E = 10^5$, Poisson ratio $\nu = 0.1$ and mass density $\rho_R = 0.001$), which are discretized by four-node isoparametric displacement-based plain strain elements. The discretization of the outer ring relies on 10×48 elements, for the inner ring 10×40 have been used (Figure 4). Note that this implies that the two meshes do not conform in the initial configuration.

The motion of the inner ring is restricted by the condition of persistent contact with the outer ring. Pure Dirichlet-type conditions are applied to fix the outer boundary of the outer ring. To get a pre-stressed initial configuration of the whole bearing, a static equilibrium problem is solved first. To this end, the initial outer diameter of the inner ring,^{||} $d_i = 80.1$, exceeds the initial inner diameter of the outer ring,^{**} $d_o = 80.0$. Accordingly, the static equilibrium problem consists of enforcing

^{||}The inner diameter is 50.

^{**}The outer diameter is 100.

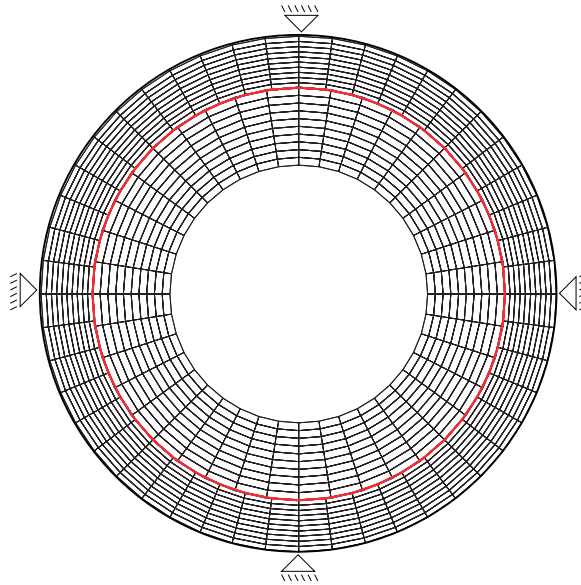


Figure 4. Initial configuration of the bearing.

(frictionless) contact between the inner and the outer ring. The static equilibrium problem is solved in one load increment.

After the solution of the equilibrium problem the transient calculation proceeds with $\Delta t = 0.01$. To start the rotation, a torque

$$T(t) = 2500f(t) \quad \text{with } f(t) = \begin{cases} \sin(2\pi t) & \text{for } 0 \leq t \leq 0,5 \\ 0 & \text{for } 0,5 < t \leq 2 \end{cases} \quad (133)$$

is acting on the inner ring. To this end, external forces are applied in tangential direction to the nodes on the inner boundary of the inner ring. Then, for $t \in (0.5, 2]$, no external loads are acting on the bearing anymore.

Figure 6 shows that for $t \geq 0.5$ the present scheme does indeed conserve the total energy for the frictionless contact problem under consideration. In addition to that, Figure 5 corroborates algorithmic conservation of the angular momentum.

It is quite remarkable that, despite the rough resolution of the contact surface in the present example, the mortar contact method, in conjunction with the energy-momentum scheme, produces astonishingly smooth results. This is in severe contrast to the NTS approach in Belytschko *et al.* [34], which, even with smoothing, requires the application of integrators with numerical dissipation.

6.2. Impact problem

The second numerical example deals with the impact of two elastic rings. Similar examples have been previously considered by Wriggers *et al.* [35] and Laursen and Love [18]. This example is especially well suited to check the algorithmic conservation properties.

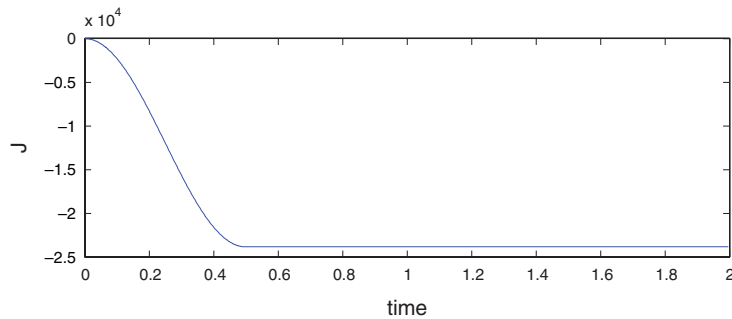


Figure 5. Total angular momentum versus time.

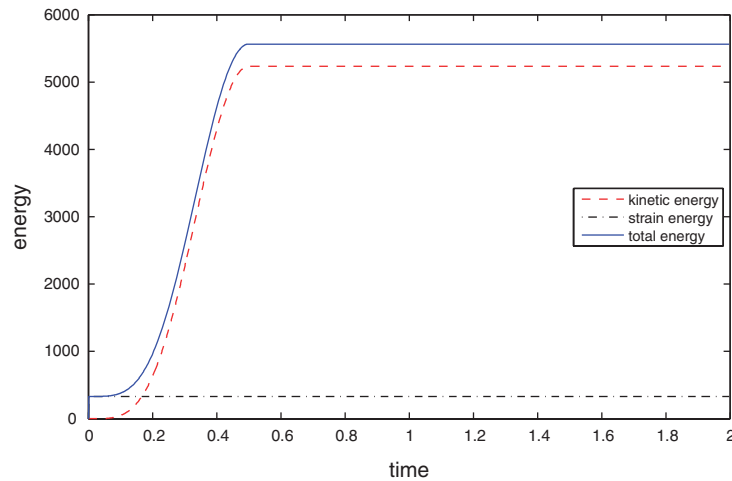


Figure 6. Energy versus time.

For the discretization of each initially circular ring, 64 isoparametric displacement-based bilinear finite elements have been used. The material behavior of both rings is assumed to be governed by the St. Venant–Kirchhoff material model with Young’s modulus $E=100$ and Poisson ratio $\nu=0.1$. The mass density of both rings is $\rho_R=0.001$. The two rings move toward each other with an initial velocity of $v_0=10$.

In the simulations documented below a time-step of $\Delta t=0.01$ has been used. To illustrate, the simulated motion snapshots of the two rings at successive points in time are depicted in Figure 7. After the initial free-flight phase contact takes place within the time interval of approximately [6, 16].

Since no external forces/torques act on the present two-body system the total linear momentum as well as the total angular momentum are conserved quantities. These momenta are indeed conserved by the proposed algorithm, see Figure 8 where the total angular momentum is displayed. Furthermore, algorithmic conservation of the total energy can be observed from Figure 9.

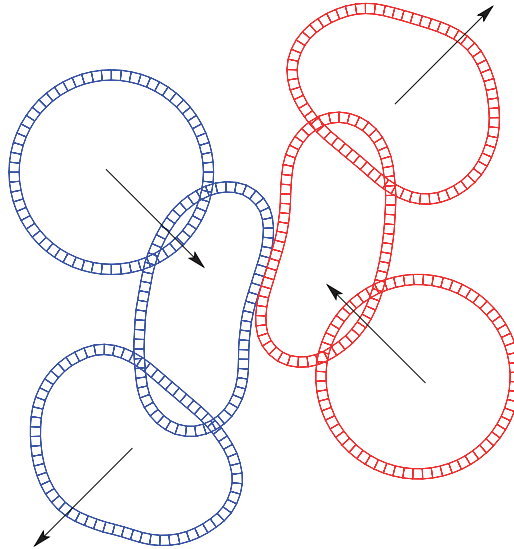


Figure 7. Snapshots of the motion.

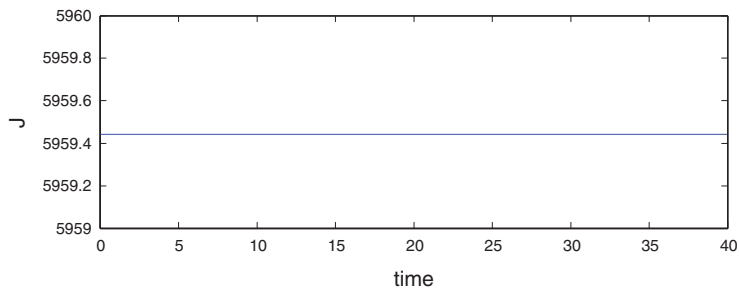


Figure 8. Total angular momentum versus time.

Table II contains a comparison of the maximum condition number of the iteration matrix for both solution schemes under consideration, namely solution of the original saddle point system or application of the discrete null space method as described in Section 5. It can be observed that application of the discrete null space method yields a condition number, which is independent of the time-step. In contrast to that, the condition number of the original saddle point system deteriorates if the time-step is decreased.

We finally remark that for the present impact example the results furnished by the mortar contact formulation are practically indistinguishable from those of the NTS method presented in Betsch and Hesch [3]. In both cases the proposed energy-momentum scheme exhibits remarkable numerical stability properties.

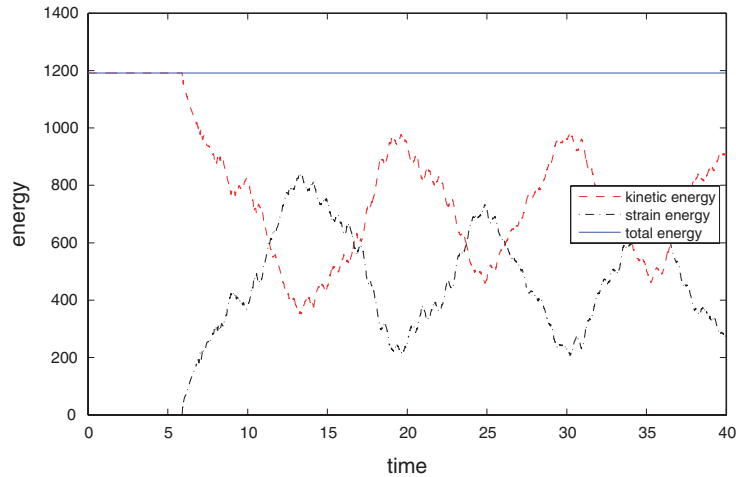


Figure 9. Energy versus time.

Table II. Comparison of the condition number of the iteration matrix.

Δt	Saddle point problem	Discrete nullspace method
10^{-1}	72	5.8×10^3
10^{-2}	2.6×10^2	1.3×10^3
10^{-3}	5.7×10^4	1.5×10^3
10^{-4}	5.2×10^7	1.5×10^3
10^{-5}	5.2×10^{10}	1.5×10^3

7. CONCLUSIONS

In this work, we have presented a new formulation of mortar contact constraints in terms of quadratic invariants. Our approach has been guided by our previous developments in the context of the NTS method presented in Betsch and Hesch [3]. Accordingly, our main aim was the design of an energy-momentum scheme by applying the notion of a discrete gradient to the evaluation of the discrete contact forces. This approach requires a specific formulation of the mortar contact constraints, which is invariant under both translations and rotations. Indeed, the description of the mortar contact constraints in terms of the invariants presented in Section 3 verifies the desired invariance properties of the semi-discrete formulation. To the best of our knowledge, the present approach yields the first mortar contact formulation that inherits rotational invariance from the underlying continuous formulation.

The aforementioned invariance properties of the semi-discrete contact description lay the foundation for the energy-momentum scheme presented in Section 4. The mortar contact formulation combined with the conserving time discretization leads to a numerical method that exhibits remarkable stability and robustness properties. In fact, the numerical example presented in Section 6.1

indicates that the present approach is a substantial improvement on the classical NTS method, even if smoothing techniques are applied.

The proposed implementation relies on an iterative solution procedure embedded into an active set algorithm. Owing to the use of Lagrange multipliers for the enforcement of the mortar contact constraints, in each Newton iteration a saddle point system has to be solved. To obtain a size-reduction along with an improved conditioning of the system to be solved the discrete null space method has been applied (Section 5). If the underlying saddle point system is symmetric, e.g. in the case of static equilibrium problems, the symmetry can be retained in the size-reduced system (Section 5.1). Similar to previously developed energy-momentum schemes, the present time discretization yields an unsymmetric iteration matrix. Accordingly, in the case of transient problems, a generalized saddle point system has to be solved. In addition to the elimination of the Lagrange multipliers, the discrete null space method yields an iteration matrix whose condition number is independent of the time-step. That is, the conditioning does not deteriorate if the time-step is decreased.

The developments presented herein are restricted to the planar case and space discretizations relying on linear finite elements. However, the extension to the three-dimensional setting and higher-order finite elements should be possible. Rotational invariance of the mortar contact constraints along with conservation of the angular momentum are probably even more crucial in three-dimensional applications. Furthermore, friction effects play an important role in practical applications and should be included in future work. It is expected that conserving schemes provide a good basis for the inclusion of friction effects, facilitating the development of energy-consistent schemes.

APPENDIX A: LINEARIZATION OF THE MORTAR CONTACT CONSTRAINTS

In this appendix we outline the linearization of the discrete contact forces. In particular, we focus on the element contributions to the discrete gradient given by (80). For simplicity of exposition set $\tilde{\mathbf{q}} = \mathbf{q}_{\text{seg}}$, so that (80) can be written as

$$\begin{aligned} \bar{\nabla} \Phi_e^\alpha &= \bigcup_{\text{seg}} D\pi(\tilde{\mathbf{q}}_{n+\frac{1}{2}})^T \bar{\bar{\nabla}} \tilde{\Phi}_{\text{seg}}^\alpha(\boldsymbol{\pi}_n, \boldsymbol{\pi}_{n+1}) \\ &= \bigcup_{\text{seg}} \sum_{i=1}^5 \nabla \pi_i(\tilde{\mathbf{q}}_{n+\frac{1}{2}}) \bar{\bar{\nabla}}_{\pi_i} \tilde{\Phi}_{\text{seg}}^\alpha(\boldsymbol{\pi}_n, \boldsymbol{\pi}_{n+1}) \\ &= \bigcup_{\text{seg}} \mathbf{g}_{\text{seg}}(\tilde{\mathbf{q}}_n, \tilde{\mathbf{q}}_{n+1}) \end{aligned} \tag{A1}$$

The linearization of the segment contributions in (A1)₃ may be written as

$$\Delta \mathbf{g}_{\text{seg}} = \mathbf{K}_{\text{seg}} \Delta \tilde{\mathbf{q}}_{n+1} \tag{A2}$$

where the 8×8 matrix \mathbf{K}_{seg} is given by

$$\begin{aligned} \mathbf{K}_{\text{seg}} &= D\pi(\tilde{\mathbf{q}}_{n+\frac{1}{2}})^T \frac{\partial}{\partial \boldsymbol{\pi}_{n+1}} (\bar{\bar{\nabla}} \tilde{\Phi}_{\text{seg}}^\alpha(\boldsymbol{\pi}_n, \boldsymbol{\pi}_{n+1})) D\pi(\tilde{\mathbf{q}}_{n+1}) \\ &\quad + \frac{1}{2} \sum_{i=1}^5 \bar{\bar{\nabla}}_{\pi_i} \tilde{\Phi}_{\text{seg}}^\alpha(\boldsymbol{\pi}_n, \boldsymbol{\pi}_{n+1}) \nabla^2 \pi_i(\tilde{\mathbf{q}}_{n+\frac{1}{2}}) \end{aligned} \tag{A3}$$

Since the invariants $\pi_i(\tilde{\mathbf{q}})$, $i = 1, \dots, 5$ are quadratic, the associated Hessians $\nabla^2\pi_i(\tilde{\mathbf{q}})$ are constant. In particular, with regard to the definition of the invariants in (61) and (71), we obtain

$$\begin{aligned} \nabla\pi_1(\tilde{\mathbf{q}}) &= \begin{bmatrix} -2\mathbf{a} \\ 2\mathbf{a} \\ \mathbf{0} \\ \mathbf{0} \end{bmatrix}, \quad \nabla\pi_2(\tilde{\mathbf{q}}) = \begin{bmatrix} -\mathbf{a} - (\mathbf{q}_1^{(2)} - \mathbf{q}_1^{(1)}) \\ (\mathbf{q}_1^{(2)} - \mathbf{q}_1^{(1)}) \\ \mathbf{a} \\ \mathbf{0} \end{bmatrix}, \quad \nabla\pi_3(\tilde{\mathbf{q}}) = \begin{bmatrix} -\mathbf{a} - (\mathbf{q}_2^{(2)} - \mathbf{q}_1^{(1)}) \\ (\mathbf{q}_2^{(2)} - \mathbf{q}_1^{(1)}) \\ \mathbf{0} \\ \mathbf{a} \end{bmatrix} \\ \nabla\pi_4(\tilde{\mathbf{q}}) &= \begin{bmatrix} \Lambda(-2\mathbf{a} - 2\mathbf{q}_1^{(1)} + \mathbf{q}_1^{(2)} + \mathbf{q}_2^{(2)}) \\ \Lambda(-2\mathbf{q}_1^{(1)} + \mathbf{q}_1^{(2)} + \mathbf{q}_2^{(2)}) \\ -\Lambda\mathbf{a} \\ -\Lambda\mathbf{a} \end{bmatrix}, \quad \nabla\pi_5(\tilde{\mathbf{q}}) = \begin{bmatrix} \Lambda(\mathbf{q}_1^{(2)} - \mathbf{q}_2^{(2)}) \\ -\Lambda(\mathbf{q}_1^{(2)} - \mathbf{q}_2^{(2)}) \\ \Lambda\mathbf{a} \\ -\Lambda\mathbf{a} \end{bmatrix} \end{aligned} \tag{A4}$$

where the abbreviation $\mathbf{a} = \mathbf{q}_2^{(1)} - \mathbf{q}_1^{(1)}$ has been used. Furthermore,

$$\begin{aligned} \nabla^2\pi_1(\tilde{\mathbf{q}}) &= \begin{bmatrix} 2\mathbf{I} & -2\mathbf{I} & \mathbf{0} & \mathbf{0} \\ -2\mathbf{I} & 2\mathbf{I} & \mathbf{0} & \mathbf{0} \\ \mathbf{0} & \mathbf{0} & \mathbf{0} & \mathbf{0} \\ \mathbf{0} & \mathbf{0} & \mathbf{0} & \mathbf{0} \end{bmatrix} \\ \nabla^2\pi_2(\tilde{\mathbf{q}}) &= \begin{bmatrix} \mathbf{I} & \mathbf{0} & -\mathbf{I} & \mathbf{0} \\ -\mathbf{I} & \mathbf{0} & \mathbf{I} & \mathbf{0} \\ \mathbf{0} & \mathbf{0} & \mathbf{0} & \mathbf{0} \\ \mathbf{0} & \mathbf{0} & \mathbf{0} & \mathbf{0} \end{bmatrix} + \begin{bmatrix} \mathbf{I} & -\mathbf{I} & \mathbf{0} & \mathbf{0} \\ \mathbf{0} & \mathbf{0} & \mathbf{0} & \mathbf{0} \\ -\mathbf{I} & \mathbf{I} & \mathbf{0} & \mathbf{0} \\ \mathbf{0} & \mathbf{0} & \mathbf{0} & \mathbf{0} \end{bmatrix} \\ \nabla^2\pi_3(\tilde{\mathbf{q}}) &= \begin{bmatrix} \mathbf{I} & \mathbf{0} & \mathbf{0} & -\mathbf{I} \\ -\mathbf{I} & \mathbf{0} & \mathbf{0} & \mathbf{I} \\ \mathbf{0} & \mathbf{0} & \mathbf{0} & \mathbf{0} \\ \mathbf{0} & \mathbf{0} & \mathbf{0} & \mathbf{0} \end{bmatrix} + \begin{bmatrix} \mathbf{I} & -\mathbf{I} & \mathbf{0} & \mathbf{0} \\ \mathbf{0} & \mathbf{0} & \mathbf{0} & \mathbf{0} \\ \mathbf{0} & \mathbf{0} & \mathbf{0} & \mathbf{0} \\ -\mathbf{I} & \mathbf{I} & \mathbf{0} & \mathbf{0} \end{bmatrix} \\ \nabla^2\pi_4(\tilde{\mathbf{q}}) &= \begin{bmatrix} 2\Lambda & \mathbf{0} & -\Lambda & -\Lambda \\ -2\Lambda & \mathbf{0} & \Lambda & \Lambda \\ \mathbf{0} & \mathbf{0} & \mathbf{0} & \mathbf{0} \\ \mathbf{0} & \mathbf{0} & \mathbf{0} & \mathbf{0} \end{bmatrix} + \begin{bmatrix} 2\Lambda & -2\Lambda & \mathbf{0} & \mathbf{0} \\ \mathbf{0} & \mathbf{0} & \mathbf{0} & \mathbf{0} \\ -\Lambda & \Lambda & \mathbf{0} & \mathbf{0} \\ -\Lambda & \Lambda & \mathbf{0} & \mathbf{0} \end{bmatrix} \end{aligned} \tag{A5}$$

$$\nabla^2 \pi_5(\tilde{\mathbf{Q}}) = \begin{bmatrix} \mathbf{0} & \mathbf{0} & \Lambda & -\Lambda \\ \mathbf{0} & \mathbf{0} & -\Lambda & \Lambda \\ \mathbf{0} & \mathbf{0} & \mathbf{0} & \mathbf{0} \\ \mathbf{0} & \mathbf{0} & \mathbf{0} & \mathbf{0} \end{bmatrix} + \begin{bmatrix} \mathbf{0} & \mathbf{0} & \mathbf{0} & \mathbf{0} \\ \mathbf{0} & \mathbf{0} & \mathbf{0} & \mathbf{0} \\ \Lambda & -\Lambda & \mathbf{0} & \mathbf{0} \\ -\Lambda & \Lambda & \mathbf{0} & \mathbf{0} \end{bmatrix}$$

where \mathbf{I} and $\mathbf{0}$ denote the 2×2 identity and zero matrix, respectively. It remains to determine the 5×5 matrix $\partial(\overline{\nabla \tilde{\Phi}}_{\text{seg}}^\alpha) / \partial \pi_{n+1}$ in (A3). This is a tedious but straightforward calculation starting from the discrete derivative of the constraints defined by (81).

REFERENCES

1. Gonzalez O. Time integration and discrete Hamiltonian systems. *Journal of Nonlinear Sciences* 1996; **6**:449–467.
2. Gonzalez O. Mechanical systems subject to holonomic constraints: differential-algebraic formulations and conservative integration. *Physica D* 1999; **132**:165–174.
3. Betsch P, Hesch C. Energy-momentum conserving schemes for frictionless dynamic contact problems. Part I: NTS method. In *IUTAM Symposium on Computational Methods in Contact Mechanics*, Wriggers P, Nackenhorst U (eds). IUTAM Bookseries, vol. 3. Springer: Berlin, 2007; 77–96.
4. Laursen TA. *Computational Contact and Impact Mechanics*. Springer: Berlin, 2002.
5. Wriggers P. *Computational Contact Mechanics* (2nd edn). Springer: Berlin, 2006.
6. McDevitt TW, Laursen TA. A mortar-finite element formulation for frictional contact problems. *International Journal for Numerical Methods in Engineering* 2000; **48**:1525–1547.
7. Puso MA, Laursen TA. A mortar segment-to-segment contact method for large deformation solid mechanics. *Computer Methods in Applied Mechanics and Engineering* 2004; **193**:601–629.
8. Hüeber S, Wohlmuth BI. A primal–dual active set strategy for non-linear multibody contact problems. *Computer Methods in Applied Mechanics and Engineering* 2005; **194**:3147–3166.
9. Yang B, Laursen TA, Meng X. Two dimensional mortar contact methods for large deformation frictional sliding. *International Journal for Numerical Methods in Engineering* 2005; **62**:1183–1225.
10. Fischer KA, Wriggers P. Frictionless 2d contact formulations for finite deformations based on the mortar method. *Computational Mechanics* 2005; **36**:226–244.
11. Brunssen S, Schmid F, Schäfer M, Wohlmuth B. A fast and robust iterative solver for nonlinear contact problems using a primal–dual active set strategy and algebraic multigrid. *International Journal for Numerical Methods in Engineering* 2007; **69**:524–543.
12. Hartmann S, Brunssen S, Ramm E, Wohlmuth BI. Unilateral non-linear dynamic contact of thin-walled structures using a primal–dual active set strategy. *International Journal for Numerical Methods in Engineering* 2007; **70**(8):883–912.
13. Puso MA, Laursen TA, Solberg J. A segment-to-segment mortar contact method for quadratic elements and large deformations. *Computer Methods in Applied Mechanics and Engineering* 2008; **197**:555–566.
14. Géradin M, Cardona A. *Flexible Multibody Dynamics: A Finite Element Approach*. Wiley: New York, 2001.
15. Leyendecker S, Betsch P, Steinmann P. The discrete null space method for the energy consistent integration of constrained mechanical systems. Part III: flexible multibody dynamics. *Multibody System Dynamics* 2008; **19**(1–2):45–72.
16. Laursen TA, Chawla V. Design of energy conserving algorithms for frictionless dynamic contact problems. *International Journal for Numerical Methods in Engineering* 1997; **40**:863–886.
17. Armero F, Petőcz E. Formulation and analysis of conserving algorithms for frictionless dynamic contact/impact problems. *Computer Methods in Applied Mechanics and Engineering* 1998; **158**:269–300.
18. Laursen TA, Love GR. Improved implicit integrators for transient impact problems—geometric admissibility within the conserving framework. *International Journal for Numerical Methods in Engineering* 2002; **53**:245–274.
19. Hauret P, Le Tallec P. Energy-controlling time integration methods for nonlinear elastodynamics and low-velocity impact. *Computer Methods in Applied Mechanics and Engineering* 2006; **195**:4890–4916.
20. Haikal G, Hjelmstad KD. A finite element formulation of non-smooth contact based on oriented volumes for quadrilateral and hexahedral elements. *Computer Methods in Applied Mechanics and Engineering* 2007; **196**:4690–4711.

21. Hughes TJR. *The Finite Element Method*. Dover: New York, 2000.
22. Simo JC, Wriggers P, Taylor RL. A perturbed Lagrangian formulation for the finite element solution of contact problems. *Computer Methods in Applied Mechanics and Engineering* 1985; **50**:163–180.
23. Papadopoulos P, Taylor RL. A mixed formulation for the finite element solution of contact problems. *Computer Methods in Applied Mechanics and Engineering* 1992; **94**:373–389.
24. Zavarise G, Wriggers P. A segment-to-segment contact strategy. *Mathematical and Computational Modelling* 1998; **28**:497–515.
25. Truesdell C, Noll W. *The Non-linear Field Theories of Mechanics*. Springer: Berlin, 2004.
26. Antman SS. *Nonlinear Problems of Elasticity* (2nd edn). Springer: Berlin, 2005.
27. Simo JC, Tarnow N. The discrete energy-momentum method. Conserving algorithms for nonlinear elastodynamics. *Zeitschrift für Angewandte Mathematik und Physik (ZAMP)* 1992; **43**:757–792.
28. Betsch P. The discrete null space method for the energy consistent integration of constrained mechanical systems. Part I: holonomic constraints. *Computer Methods in Applied Mechanics and Engineering* 2005; **194**:5159–5190.
29. Benzi M, Golub GH, Liesen J. Numerical solution of saddle point problems. *Acta Numerica* 2005; **14**:1–137.
30. Krause R, Wohlmuth BI. Nonconforming domain decomposition techniques for linear elasticity. *East–West Journal of Numerical Mathematics* 2000; **8**(3):177–206.
31. Ainsworth M. Essential boundary conditions and multi-point constraints in finite element analysis. *Computer Methods in Applied Mechanics and Engineering* 2001; **190**:6323–6339.
32. Muñoz JJ. Modelling unilateral frictionless contact using the null-space method and cubic B-spline interpolation. *Computer Methods in Applied Mechanics and Engineering* 2008; **197**:979–993.
33. Chow E, Manteuffel TA, Tong C, Wallin BK. Algebraic elimination of slide surface constraints in implicit structural analysis. *International Journal for Numerical Methods in Engineering* 2003; **57**:1129–1144.
34. Belytschko T, Daniel WJT, Ventura G. A monolithic smoothing-gap algorithm for contact–impact based on the signed distance function. *International Journal for Numerical Methods in Engineering* 2002; **55**:101–125.
35. Wriggers P, Van TV, Stein E. Finite element formulations of large deformation impact–contact problems with friction. *Computers and Structures* 1990; **37**:319–331.